LBL--13935

DE82 018803

LBL-13935

DENSITY AND POTENTIAL MEASUREMENTS IN AN INTENSE ION-BEAM-GENERATED PLASMA

Norman Edwin Abt

Ph.D. Thesis

Lawrence Berkeley Laboratory
University of California
Berkeley, CA 94720

May, 1982

This work was supported by the Director, Office of Energy Research, Office of Fusion Energy, Development and Technology Division, of the U.S. Department of Energy under Contract No. DE-AC03-76SF00098.

Density and Potential Measurements in an Intense Ion Beam-generated Plasma

Norman E. Abt

Lawrence Berkeley Laboratory
University of California
Berkeley, CA 94720

ABSTRACT

Neutral beams are created by intense large area ion beams which are neutralized in a gas cell. The interaction of the beam with the gas cell creates a plasma. Such a plasma is studied here. The basic plasma parameters, electron temperature, density, and plasma potential, are measured as a function of beam current and neutral gas pressure. These measurements are compared to a model based on the solution of Poisson's equation. Because of the cylindrical geometry the equation cannot be solved analytically. Details of the numerical method are presented. Three refinements to existing models have been added. (1) The beam creates ions by charge exchange as well as by ionization. These ions are created without matching electrons and generate a new current to the walls. This raises the plasma potential. (2) In the ionization process most of the ions are born at rest but some of the ions are born through a molecular dissociation process which provides them with substantial energy. This energy affects the flow and density of the ions. (3) Electrons are trapped in the potential well of the system. Their distribution will be truncated by the well and the usual Boltzmann relation for the density variation with potential will be

altered slightly. Analytical expressions for these effects are obtained and included in the computer generated solution. The model and data are in good agreement only when locally determined beam current profiles are used in the solution. These profiles are broader than those determined from beam dump calorimetry.

TABLE OF CONTENTS

ACKNOWLEDGMENTS

It seems everyone in the group contributed to this work and I would specifically like to thank several of them. Wulf Kunkel, Bill Cooper and Mike Vella spent many hours discussing physics with me. Rick Steele helped me keep my computer programs running and Warren Stearns was always there with a solution to every problem. I benefited greatly from contact with other graduate students particularly Glenn Rankin and Bart Billard. I can't thank enough Gary Guethlein who helped me run the equipment and take the data and looked over my shoulder constantly wanting explanation of the results. Allan Kaufman helped me put this document in good form. And it would have been a long time until anyone ever saw it without the typing and extra effort of Tina Aitkens and Martha Dueñas.

This work was supported by the Director, Office of Energy Research, Office of Fusion Energy, Development and Technology Division, of the U. S. Department of Energy under Contract No. DE-AC03-76SF00098.

Glossary of Symbols

A_p	Surface area of the Langmuir probe
A_s	Surface area of the neutralizer walls
e	Charge on an electron
E	Energy, constant of the motion
E_n	Average energy of an electron created by beam ionization
E_o	Energy on an ion created by dissociation
f	Fraction of electrons created with more energy than the potential well, distribution function
G	Ion generation rate
h	Step size in computer solution
i_b	Beam current collected by probe
i_{b+s}	Current due to beam arriving and secondary emission electrons leaving the probe
i_e	Collected electron current
i_i	Collected ion current
J	Angular momentum
m_e	Electron mass
m_i	Ion mass
n_b	Density of beam ions
n_{cx}	Density of ion created by charge exchange
n_e	Electron density
n_{ef}	Density of electron created with more energy than the potential well
n_{es}	Density of electron created with less energy than the potential well
n_{ew}	Density of electrons that originate at the walls
n_g	Density of the neutral gas
n_i	Ion density
n_{if}	Density of ions created through dissociation process
n_{is}	Density of ions created at rest

P	Unknown power input to plasma
r	Cylindrical coordinate
r_w	Radius of the wall
r_o	Normalizing scale length
R	Ratio of beam density to electron density
R_e	Electron loss rate
R_{ef}	Fast electron loss rate
R_{es}	Slow electron loss rate
R^i	Ionization rate
R_i	Ion loss rate
t	Computer solution variable
T_e	Electron temperature, in energy units
U	Effective potential
v	Particle velocity
v_b	Beam velocity
$\bar{v}$	Average electron velocity
v_o	Velocity of ion created by dissociation
V_b	Volume of the beam
y	Dimensionless radial coordinate
δn	Increment of density
λ_d	Debye length
ρ	Radial coordinate, source point
ϕ	Potential
$\bar{\phi}$	Average potential
χ	Dimensionless potential

LIST OF FIGURE CAPTIONS

CHAPTER 1

INTRODUCTION

Much of the current success of the fusion program is due to the development of neutral beams for plasma heating. Neutral beam sources are currently capable of producing 65 amps at 120 keV for 1.5 seconds and higher power, longer operating ones are being developed. In spite of, or perhaps because of, the rapid achievement of various design goals, certain areas of the beam system operation have not been studied. In addition certain operating parameters are not well understood.

In particular the measured divergence of the beams is larger than that calculated from the ion optics of the accelerator.[1] The divergence is an important design parameter in building a fusion device. The neutral beam is delivered to the target plasma through a hole in the side of the containment vessel. Magnet windings, radiation shielding and vacuum wall requirements combine to put an upper limit on the size of any opening. The divergence tends to set a lower limit. Most of the beam power must go through the opening and not deposit much energy on the edges where it will damage the wall. In present devices there is no problem but as fusion devices become larger and as the need arises to protect the source from the radiation created in the fusion plasma, the beam sources are moved farther away from the target requiring smaller divergence.

Another concern involves the neutral gas target thickness in the neutralizer. Measurements of the neutralized fraction of ions indicate a thinner target than expected.[2] This may require a greater gas input and more pumping to remove the gas. The pumping could greatly affect the cost of the system. The need for additional pumping may also increase the size, and force the sources to be moved still further away. The increased divergence and decreased gas density may be due to some process in the neutralizer.

Few measurements have been made on the plasma in the neutralizer. It is the purpose of this work, first, to provide a collection of measurements describing the plasma in the neutralizer and, second, to begin to explain those measurements. The explanation has been divided into two parts, the particle balance and the energy balance. Only the particle balance is explained in this thesis although the foundation of the energy balance is laid out.

This experiment was done on a neutral-beam line shown schematically in Fig. 1.1. Neutral gas is fed into the source where a hot filament discharge creates a plasma. The entire source is raised to high positive voltage. Ions flow out slots in the source and are accelerated as they fall down to ground potential through a set of focusing grids. Neutral gas also flows out of the slots and fills the neutralizer. In the neutralizer the beam ions collide with the neutral gas and frequently undergo charge exchange. The fast ions become fast neutrals. Some beam neutrals can undergo another collision and be converted back to an ion so for a given amount of neutral gas traversed, the beam will consist of a certain percentage

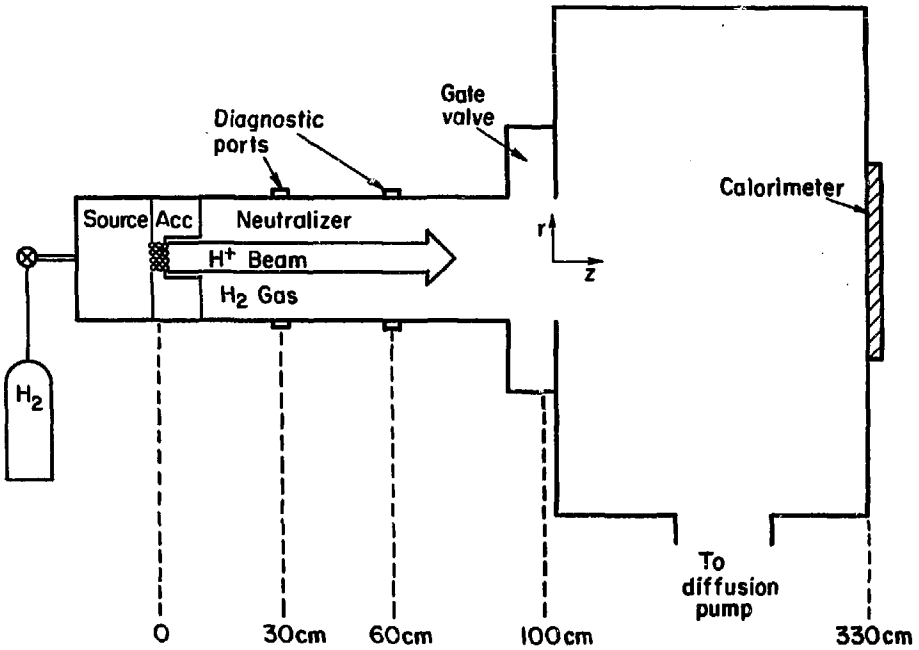
Diagnostic ports
Gate valve
Calorimeter
Source
Acc
Neutralizer
H+ Beam
H2 Gas
r
z
H2
0
30cm
60cm
100cm
To diffusion pump
330cm

XBL 824-3758

of neutrals and a certain percentage of ions. This mixed beam reaches a region of good vacuum past the gate valve where the mix stops changing and then proceeds to strike the calorimeter where it deposits its energy.

In this experiment we are examining the plasma created by the beam in the neutralizer. In addition to the ions created by the charge exchange, beam collisions will ionize the gas creating ion and electron pairs. This plasma is unusual in that the beam creating it is at the same time fairly intense (~ .25A/cm^2) and large area (50cm^2). Also there is an area of no plasma production surrounding the beam. The model we are using to explain the particle balance is basically the Tonks-Langmuir plasma sheath equation.[3] This equation has been treated several times in the past with different ionization sources and in different configurations. Parker[4] solved it numerically in cylindrical geometry with thermal electrons responsible for the ionization. Dunn and Self[5], working in planar geometry, presented a numerical solution where an electron beam of finite width was the ionization source. They neglected the space charge of the beam in that solution but included it in an expansion solution. Other expansion solutions were presented by Self[6] covering all three geometries and assuming either uniform or electron thermal ionization. The same cases excluding spherical geometry were treated using fluid equations based on moments of the Boltzmann equation by King and Shaw.[7] More recently Hooper et.al.[8] used the fluid approach together with ionization by positive or negative ion beams to describe a similar

plasma. They assumed quasineutrality throughout and so could not include the sheath in their solution. In our analysis of this plasma we include three effects not previously contained in any discussion of beam generated plasmas. First, there are ions created without accompaning electrons i.e., those created in the charge exchange. These produce a net current to the wall whereas in most plasmas the net current is zero. Second, not all ions are born at rest. In the ionization process some H_2^+ ions dissociate producing fast H^+ ions. These may alter the ion den- sity and modify the ion flow to the wall. And third, the electrons are trapped in a potential well which will truncate their distribution. This will affect the electron density variation with potential. We solve the full equation numerically.

Two papers address the energy balance, Gabovich et.al.[9] and Holmes.[10] The underlying physics in both is the same as is pesented here but both papers make assumptions in order to develop a more detailed theory with which we do not agree.

The thesis is organized as follows. Chapter 2 describes the basic processes and gives a model for the plasma ion flow. Chapter 3 describes the neutral-beam line and lists the diagnostics used. A more detailed description of the diagnostics is found in the appendices. There follow in Chapters 4 and 5 results of the various measurements made and a comparison to the model.

CHAPTER 2

THEORY

A. Neutralizer Plasma

This section presents a model for the plasma created by an ion beam passing through neutral background gas such as is found in the neutralizer of a neutral beamline. The problem has been discussed in several articles. The description here is primarily an elaboration and generalization of the treatment presented by Gabovich et. al.[9] We will begin by listing the different types of ions and electrons found in this system. The types are distinguished by the source of those particular particles.

The basic creation process involved is fast ions (keV) striking gas molecules and creating electrons and ions. (A simple calculation in Appendix D shows that the thermal ionization is not important for our particular case.) We will define three types of electrons: fast, slow, and wall. The fast and slow electrons are created by the beam ionizing the background gas. This ionization mechanism contributes considerable energy to the electrons. For 50 keV incident H^+ the electrons will average 22 eV.[11] The plasma has a potential well that tends to confine electrons. We define the fast electrons (n_{ef}) as those created with more energy than the well potential so that they escape immediately and define the slow electrons (n_{es}) as those with less energy which will then be trapped and require additional energy to escape. The wall electrons (n_{ew}) are those created on any of the surfaces around

the plasma and fall into the potential well. These have enough energy to immediately reach the wall on the other side but if they undergo a small scatter or reach the other side at an angle less than normal they will not have sufficient velocity directed along the potential gradient to escape, and they tend to be trapped.

There are four types of ions. First there are the beam ions (n_{ib}). These are at high speed, many keV, and create the rest of the ions through collisions with the neutral gas. Two kinds of collisions are important, ionization and charge exchange. Ionization can produce two types of ions, ions at rest (n_{is}) and, in ionizations that are accompanied by dissociation, fast ions (n_{if}) with on the order of 8 eV for H. The charge exchange process produces only ions at rest (n_{cx}). Each beam ion can undergo only one charge exchange collision. After that the newly created beam neutral can be ionized and undergo another charge exchange but since this produces an electron and a slow ion pair this multiple process is considered to be part of the ionization process.

Having identified the types of particles, we will discuss the particle and energy balance in steady state. Three rates must be equal. These are the ionization rate, R^i, the electron loss rate, R_e, and the ion loss rate, R_i.

$$R^i = n_b \, v_b \, n_g \, \sigma \, V_b$$

$$R_i = \langle n_i \, v_{is} \rangle \, A_s$$

where n_g is the neutral gas density, v_b is the velocity of the beam, V_b is the volume of the beam, v_{is} is the average velocity of escaping ions and A_s is the surface area of the boundary of the

system assumed to be cylindrical. We have assumed the ions escape radially. Note that the charge exchange ions are not included. (From the cross section data we see that fast ions are created only 1/6 as often as slow ions so for the time being we will neglect them.)

The expression for the electron loss rate is not as obvious. Let us define f as the fraction of the ionization electrons that are fast. These are lost as fast as they are created so their rate is $R_{ef}=fR^i$. The fraction considered fast will depend on the potential well depth and the nature of the electron energy distribution at birth. We assume the slow electrons are trapped and tend to a maxwellian. Their loss rate will depend on the density, temperature, and potential well depth

$$R_e = R_{ef} + R_{es} = fR^i + \frac{1}{4}\bar{v}_e\, n_{eso}\, e^{-e\phi/Te}\, A_s$$

where $\bar{v}_e$ is the mean electron velocity, n_{eso} is the density on axis and ϕ is the potential well depth. T_e is the electron temperature in units of electron volts. From the temperature and potential dependence the particle balance is coupled to the energy balance.

Before discussing the energy balance, it is important to realize that the energy of this system is contained in two parts. There is the thermal energy of the plasma and there is the potential energy of the electrostatic well. When a particle leaves the system it will always carry some kinetic energy out with it but as it leaves

it may add or substract potential energy depending on the sign of the charge. With this in mind, we now consider the energy sources and sinks in this system. The fast electrons give energy to the system. They are slowed down as they climb out of the potential well, giving their kinetic energy to the plasma. The slow electrons also give their kinetic energy to the plasma but when they leave the system by rising over the potential barrier they carry out approximately one T_e with each electron. The ions are the main loss. They are accelerated by the potential and carry out kinetic energy equal to the potential where they were created. Much of this loss is exactly cancelled by the energy contributed by the fast electrons. Consider a fast electron and ion pair being created at some point in the well where the value of the potential is ϕ. The electron gives energy $e\phi$ to the system as it escapes and the ion takes energy $e\phi$ with it to the wall, exactly cancelling each other. The only ions that require extra energy are those born in conjunction with a slow electron and even then they only need that amount of additional energy that it would have taken to get the slow electron out of the well.

It is important to note two items that are not part of the energy balance, charge exchange ions and electrons from the walls. The charge exchange ions are not involved in the energy balance. As the ion beam enters the plasma it runs up the potential hill for positive charges slowing the beam down by the small amount $e\phi$. The charge exchange ions then carry the amount $e\phi$ to the wall, this energy coming directly from the beam kinetic energy and not

involving the plasma, i.e., the neutral beam particle's energy is less than that of the original ion by exactly the amount $e\phi$.

The electrons from the wall do not carry net energy into the system. They become part of the trapped electron population for a time but they do not contribute energy by falling into the potential well. They are similar to the charge exchange ions in that they enter from ground potential and later return to ground potential transferring no net energy in the process. They may, however, become part of the trapped thermal plasma and carry out one T_e when they leave.

Because of the slow electrons there is need of an energy input to the plasma. We will not state an explicit energy source but will introduce a formal input and see what conclusion can be drawn.

There are three unknowns in this system, T_e, ϕ, and n_e or equivalently n_i. There are also three equations, two from the ion and electron particle fluxes and one from the energy balance.

$$R^i = R_i \tag{2.1a}$$

$$n_b v_b n_g \sigma V_b = \langle n_i \, v_{is} \rangle A_s \tag{2.1b}$$

$$R^i = R_e \tag{2.2a}$$

$$n_b v_b n_g \sigma V_b = f R^i + \frac{1}{4} A_s \bar{v}_e \, n_{eo} e^{-e\phi/T_e} \tag{2.2b}$$

$$e\bar{\phi}(1-f) R_i + T_e R_{es} + T_e R_{ew} = E_n R_{es} + P_{in} \tag{2.3a}$$

Equation 2.3a can be rearranged using 2.1a, 2.2b to be,

$$e\bar{\phi} + T_e + T_e \frac{R_{ew}}{R_{es}} = E_n + \frac{P}{R_{es}} \tag{2.3b}$$

P is the unknown energy input. E_n is the average energy of a slow electron. There is a lot hidden in Eq. (3). E_n is an average that depends on the potential well depth. The energy, $e\bar{\phi}$, is not given exactly by the well depth as it would be for a square well but actually by an average over the spread in potential where the ions are created. And the energy input could be due to coulomb collisions or possibly some instability. It is not our task here to elaborate on this equation, that is the work of another thesis yet to be written (tentatively planned by Gary Guethlein). Hereafter, we will assume the temperature to be known. It is easily measured and will be used as an input to later modeling.

We can think of Eq. (2.3b) as determining T_e, Eq. (2.2b) as determining the ratio between $e\phi$ and T_e, and Eq. (2.1b) as determining n. The ion flux density, $\langle n_i \cdot v_{is} \rangle$, is a formal expression that requires a complete knowledge of the ion velocity distribution and the potential variation in space in order to evaluate. Given T_e and various beam parameters, n(r) can be solved for by computer. Similar situations have been discussed in the literature.[4,5] We will present a solution for our paticular case later. In such solutions, Eq. (2) becomes the boundary condition on the current to the wall which sets the ratio $e\phi/T_e$.

So far we have not seen any effect due to the charge exchange ions. They are not in the energy balance but they do affect the ratio $e\phi/T_e$. Several amps of current leave the accelerator and this current must return to ground somewhere. The ions that undergo no charge exchange collisions return to ground through the beam

dump. The rest of the current creates slow ions distributed along the neutralizer where they contribute to the current to the wall. Equation (1) would have an additional term on the left-hand side, the production rate of ions by charge exchange. Equation (2) is unchanged but the value of n_{eo} will, from the extra term in eq. 1, turn out to be higher which will in turn require a larger value for $e\phi$.

B. Radial model

1. *Basic Equations*

We have chosen to solve for the density and potential by the direct solution of Poisson's equation. This includes the sheath in the solution and will allow us to see the effect of the charge exchange ions on the potential barrier height. Similar calculations have been made[4,5,6,7,8] though not necessarily with our combination of cylindrical coordinates, ion beam as ionization source, and space between beam and wall.

The basic equation is Poisson's equation

$$-\nabla^2\phi = 4\pi e(n_i - n_e)$$

The ions are assumed here to be created at rest. (The next section gives the calculation for ions created with some energy.) They then free-fall to the wall accelerated by the potential. We calculate the density by first getting the density at a ring at r caused by particles created at ρ. We then integrate over all values of ρ that

contribute density to r. The continuity equation in steady state with a source term is

$$\nabla \cdot (n\vec{v}) = G(r)$$

$$\int \nabla \cdot n\vec{v}\, dV = \int n\vec{v} \cdot d\vec{s} = \int G(r)\, dV$$

The increment of density δn at r that results from a source that is non-zero only at ρ is then

$$\delta n v\, 2\pi r = 2\pi G(\rho)\, \rho d\rho$$

$$\delta n = \frac{\rho}{r} \frac{G(\rho)}{v} d\rho$$

v is given by the difference in potential between ρ and r

$$v = \sqrt{\frac{2e}{m_i}} \left(\phi(\rho) - \phi(r)\right)^{1/2}$$

Combining these and integrating over ρ gives n_i.

$$n_i(r) = \frac{1}{r} \int_0^r \frac{G(\rho)\, \rho\, d\rho}{\sqrt{\frac{2e}{m_i}} \left(\phi(\rho) - \phi(r)\right)^{1/2}} \qquad (2.4)$$

Only ρ less than or equal to r contributes to the density at r since an ion born at rest can only move to regions of lower potential.

For the electrons it is easiest to assume that they are Maxwellian and follow a Boltzmann distribution. Other distributions are considered later.

$$n_e = n_{eo}\, e^{e\phi/T_e} \tag{2.5}$$

Combining these with a term for the beam ions gives

$$-\nabla^2\phi = 4\pi e \left\{ \frac{1}{r} \int_0^r \frac{G(\rho)\, \rho\, d\rho}{\sqrt{\frac{2e}{m_i}}\, (\phi(\rho) - \phi(r))^{1/2}} - n_{eo}\, e^{e\phi/T_e} + n_b(r) \right\}$$

Let us introduce a few definitions.

$$n_b(r) = n_{bo}\, g(r) \qquad G(r) = \langle n_b v \rangle g(r) \qquad \lambda_d^2 = T_e/4\pi n_{eo} e^2$$

G is the production rate and is proportional to the beam density. The beam density is given by the density at the exit grid times a shape factor. At the exit g(r) is 1 across the width of the beam and zero outside the beam. Further downstream g(r) will depend on the beam divergence and the position downstream. However, the integral of g(r) is a constant and equal to the width. $\int g(r)dr = \text{width}$ This guarantees that the number of particles remains constant along the beam. Now we introduce the following dimensionless variables

$$y = r/r_o \qquad r_o \equiv \frac{n_{eo}\, (2T_e/m_i)^{1/2}}{\langle n_b\, v \rangle}$$

$$\chi = -e\phi/T_e$$

$$\beta = r_o/\lambda_d$$

$$R = n_{bo}/n_{eo}$$

We now have:

$$\frac{1}{\beta^2} \nabla^2 x = \frac{1}{y} \int_0^y \frac{g(y')\, y'\, dy'}{[x(y) - x(y')]^{1/2}} - e^{-x} + R\, g(y) \qquad (2.7)$$

Solution of this will give the potential and density along a radius. The detailed computer solution is given in Appendix B.

There is an important difference between the physical system and the computer solution. In the real world there is a given beam profile, a specific ion production rate, and a specific wall position. The plasma will be at some temperature and a specific density at the center will result from these conditions. In the computer solution the density is specified at the center and the calculation proceeds outward from there. The wall is located by some condition on the total current to the wall. In many cases that current would be zero but in our system we expect that current to be the current of ions created by charge exchange. The total ion production rate is given by the sum of charge exchange and ionization. The ionization events include electrons and the charge exchange do not. The original beam current is converted by the charge exchange events to a net current at the wall. This does not change the solution but merely changes the location of the wall and the value of the potential at the center relative to the wall.

2. Fast Ions

In collisions between protons and H_2 molecules a certain percentage of the time H_2^+ ions in high vibrational states are

produced. These ions subsequently dissociate with the ion acquiring substantial energy. At 25 keV the cross section for the fast ions is about one-sixth that of the slow ions so it may be an important contribution to the density.[12] Here we calculate the density of the fast ions following the approach of Bernstein and Rabinowitz[13] for calculating the density around a probe.

We choose a cylindrical coordinate system and do the problem in two dimensions ignoring the axial coordinate. This is consistent with the system we are studying. The density is given by

$$n = \int f \, d^2v$$

where f is the solution to the Boltzmann equation

$$\frac{df}{dt} = \vec{v} \nabla f - \frac{e}{m} \nabla \phi \cdot \nabla_v f = 0$$

The sourceless form of the Boltzmann equation can be used even though the ions come from sources because we are considering the steady state. We simply drop the source and at the source point use the distribution function which gives the same density and velocity distribution that would be found at that point. The Boltzmann equation then describes how that distribution is related to the distribution over the rest of space. The distribution function, f, is constant along a particle orbit. For orbits in a plane the general solution is then

$$f = f(E,J)$$

where E and J are the constants of the motion, energy and angular momentum. We assume we know f on a particular ring at ρ. But because of the potential a particle starting at ρ cannot reach all values of r. Corresponding to this there are no particles in certain parts of E-J space. In these regions f is zero and the problem becomes finding the bounds of this region.

We define the potential to be zero at the origin and go to minus infinity at infinite radius. Also we define the particle energy such that a particle born at ρ with zero kinetic energy has zero total energy.

$$E = 1/2\ m\ v^2(r) + e\phi(r) - e\phi(\rho)$$

$$v^2 = v_r^2 + v_\theta^2 \qquad J^2 = m^2 r^2\ v_\theta^2$$

$$E = 1/2\ mv_r^2\ (r) + J^2/2mr^2 + e\phi(r) - e\phi(\rho)$$

Now we will define a potential U(r,J)

$$U(r,J) = J^2/2mr^2 - e\phi(r) - e\phi(\rho)$$

The density has two different forms depending on whether we are evaluating the density at a point r less than or greater than the point ρ where the particles were born. All ions leaving ρ will pass through $r>\rho$ but for some E and J an ion will be unable to reach all values $r<\rho$. Figure 2 shows the potential as a function of r for

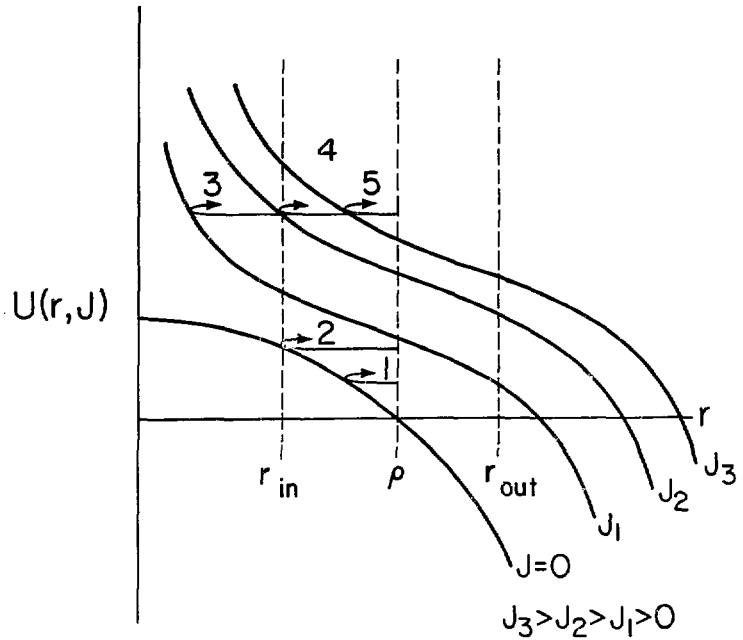

XBL 824-302

Figure 2

several values of J and several orbits. For $E < U(r_{in}, J=0)$ the particle will not reach r_{in} (r_{in}: $r < \rho$) as in orbit 1. $E = U(r_{in},0)$ is the boundary shown in orbit 2. For larger E there is a limit imposed by the angular momentum as shown by orbits 3, 4, and 5. Only when $E > U(r_{in}, J_2)$ will the particle reach r_{in}. This puts the condition on J^2

$$J^2 < 2\, m r_{in}^2 \,[E - e\phi(r_{in}) + e\phi(\rho)]$$

For r_{out} (r_{out}: $r > \rho$) all particles will arrive there but there is a limit on J for the definitions

$$J^2 \leq 2\, m_p{}^2\, E$$

Figures 3a and b, show the region of $E\text{-}J^2$ phase space to be integrated over for r_{in} and r_{out} respectively. In going from v_x, v_y to E, J

$$d^2v = \frac{dE\ \ dJ}{m[2mr^2[E - e\phi(r) + e\phi(\rho)] - J^2]^{1/2}} \quad *$$

---

* $dv_x\, dv_y = r\, d\dot{r}\, d\dot{\theta} = r\,[\frac{\partial\dot{\theta}}{\partial J}\frac{\partial\dot{r}}{\partial E} - \frac{\partial\dot{\theta}}{\partial E}\frac{\partial\dot{r}}{\partial J}]\, dE\, dJ$

$\dot{\theta} = v_\theta/r = J/mr^2$

$\frac{\partial\dot{\theta}}{\partial E} = 0$

$\frac{\partial\dot{\theta}}{\partial J} = \frac{1}{mr^2}$

$\dot{r} = V_r = [\frac{2}{m}[E - e\phi(r) + e\phi(\rho)] - \frac{J^2}{m^2r^2}]^{1/2}$

$\frac{d\dot{r}}{dE} = \left[2m\,[E - e\phi(r) + e\phi(\rho)] - J^2/r^2\right]^{-1/2}$

$dv_x\, dv_y = \frac{dE\, dJ}{m[2mr^2[E - e\phi(r) + e\phi(\rho)] - J^2]^{1/2}}$

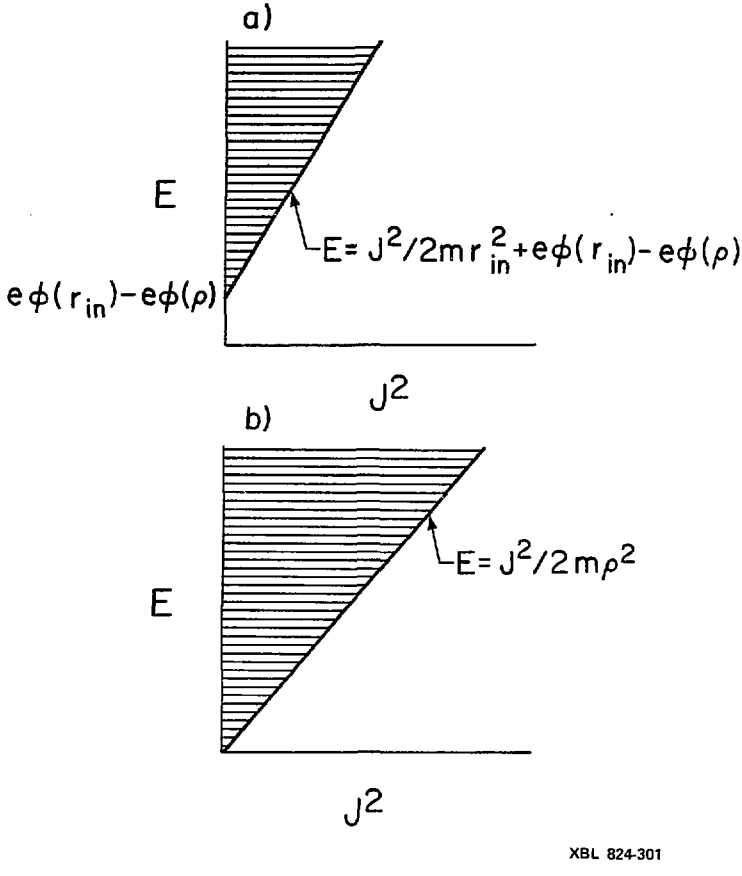
a)
E
$E = J^2/2mr_{in}^2 + e\phi(r_{in}) - e\phi(\rho)$
$e\phi(r_{in}) - e\phi(\rho)$
J^2
b)
E
$E = J^2/2m\rho^2$
J^2
XBL 824-301

Figure 3

Now $\delta n(r,\rho)$, the contribution to the density at r from a distribution at ρ, is given by

$$\delta n(r,\rho) = \int_{e\phi(r)-e\phi(\rho)}^{\infty} dE \int_0^{\left[2m r^2[E - e\phi(r) + e\phi(\rho)]\right]^{1/2}} dJ \frac{f(E,J)}{m\left[2mr^2\,[E-e\phi(r) + e\phi(\rho)] - J^2\right]^{1/2}} \qquad r < \rho \tag{2.8a}$$

$$= \int_0^{\infty} dE \int_0^{(2m\rho^2\,E)^{1/2}} dJ \frac{f(E,J)}{m\left[2mr^2[E-e\phi(r) + e\phi(\rho)] - J^2\right]^{1/2}} \qquad r > \rho \tag{2.8b}$$

If we assume that f is independent of J, then δn becomes upon integration:

$$\delta n(r,\rho) = \int_0^{\infty} f(E)\, dE\, \Theta\left[E - e\phi(R) + e\phi(\rho)\right] \qquad r < \rho \tag{2.9}$$

$$\delta n(r,\rho) = \int_0^{\infty} dE\, f(E) \arcsin\left[\frac{\rho}{r}\left(\frac{E}{E - e\phi(r) + e\phi(\rho)}\right)^{1/2}\right] \qquad r > \rho$$

The fact that the density is constant for $r < \rho$ is a result of geometry. The result is reasonable as can be seen from the following argument. The density on a cylinder results from three effects. First, for decreasing radius the volume for the particles

is shrinking so the density increases as 1/r. Second, as the particles move in they slow down against the potential. Again, the density should increase this time as $\frac{1}{v}$ or $\frac{1}{(E-e\phi)^{\frac{1}{2}}}$ Third, because of the angular momentum, fewer particles can reach the inner radius. One can define a critical solid angle at ρ that sets the limit on reaching r and should be proportional to the density, δn.

In general

$$J = m\rho\sqrt{\frac{2E}{m}}\sin\theta$$

The limit on J is

$$J^2_{crit} = 2mr^2\,[E-e\phi]$$

Combining these gives

$$\theta_{crit} \propto \arcsin\left[\frac{r}{\rho}\left(\frac{E-e\phi}{E}\right)^{1/2}\right]$$

so δn is given by

$$\delta n \propto \frac{\theta_{crit}}{rv} \propto \frac{\arcsin\left[\frac{r}{\rho}\left(\frac{E-e\phi}{E}\right)^{1/2}\right]}{r(E-e\phi)^{1/2}} \simeq \text{constant}$$

for small r.

Also for $r > \rho$ the solid angle is a constant 2π so δn is given by $\delta n \propto \frac{1}{r(E-e\phi)^{\frac{1}{2}}}$, which is the limit for large r of the expression obtained earlier.

In our system, all the particle production takes place in the beam where the potential variation from the center to the edge of the beam is about T_e.[5] This is generally smaller than the energy from dissociation. It is convenient then to take f(E) to be $\delta n_0 \delta(E-E_0)$ where $E_0 > e\phi(r)$ for non zero G(r) and

$$\delta n_o = \frac{G(\rho)}{\sqrt{\frac{2\,E_o}{m}}}\, d\rho$$

We now compute the total fast ion density from all the sources.

$$n(r) = \int \delta n(r,\rho)$$

From Eqs. (2.9a) and (2.9b)

$$\delta n(r,\rho) = \frac{G(\rho)}{v_o}\, d\rho \qquad r < \rho$$

$$= \frac{G(\rho)}{v_o}\, d\rho\, \sin^{-1}\left[\frac{\rho}{r}\left(\frac{E_o}{E_o - e\phi(r) + e\phi(\rho)}\right)^{1/2}\right] \qquad r < \rho$$

where $v_o = \sqrt{\frac{2E_o}{m}}$

$$n(r) = \int_r^\infty \frac{G(\rho)}{v_o}\, d\rho + \int_0^r \frac{G(\rho)}{v_o}\, d\rho\, \sin^{-1}\left[\frac{\rho}{r}\left(\frac{E_o}{E_o - e\phi(r) + e\phi(\rho)}\right)^{1/2}\right]$$

It is convenient to rewrite this as

$$n(r) = \int_0^\infty \frac{G(\rho)}{v_o}\, d\rho + \int_0^r \frac{G(\rho)}{v_o}\, d\rho \left\{\sin^{-1}\left[\frac{\rho}{r}\left(\frac{E_o}{E_o - e\phi(r) + e\phi(\rho)}\right)^{1/2}\right] - 1\right\}$$

The first integral is a constant and the second depends only on values of the potential less than r, which makes it easier to solve on the computer.

3. Alternative electron distributions

This plasma sits in a potential well that confines electrons. Electrons with more energy than the well depth are expected to escape. This will leave us with a truncated distribution. We can use an analysis like that for the fast ions. The effective potential is shown in Fig. 4a. We will consider various values for E and J, and see which orbits exist that do not intersect the wall. The potential is defined to be zero at the origin and goes to positive infinity at infinity. A particle at r has energy no less than $E = e\phi(r)$ and if $E < e\phi(r_w)$ then no matter what J is it cannot reach the wall (orbit 1). For larger E those with larger J are trapped (orbit 2) and those with less angular momentum reach the wall (orbit 4). The lower limit on J is given by orbit 3.

$$J^2 > 2mr_w^2[E - e\phi(r_w)]$$

There is still an upper limit on J from the energy limit.

$$J^2 \leq 2mr^2[E - e\phi(r)]$$

These two limits meet at orbit 5. For $E > E_{max}$ all orbits reach the wall. Figure 4b shows the phase space. The cross hatched area contain those orbits that do not have sufficient energy to reach the wall. In the striped area electrons have sufficient energy but the angular momentum is such that the orbit does not intercept the wall. In integral form

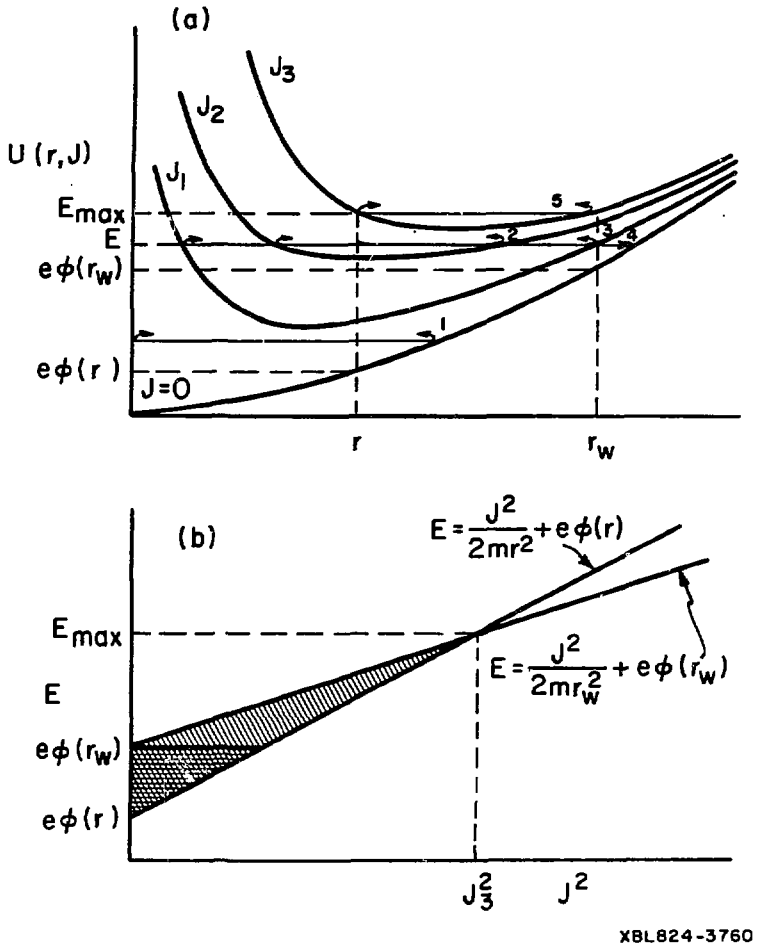
(a)
U (r,J)
J3
J2
J1
Emax
E
eφ(rw)
eφ(r)
J=0
1
2
3
4
5
r
rw
(b)
E = J²/2mr² + eφ(r)
E = J²/2mrw² + eφ(rw)
Emax
E
eφ(rw)
eφ(r)
J3²
J²
XBL824-3760

Figure 4

$$n_e(r) = I_1 + I_2$$

$$= \int_{e\phi(r)}^{e\phi(r_w)} dF \int_0^{\sqrt{2m}\, r(E-e\phi(r))^{1/2}} dJ \frac{f(E,J)}{m\left[2mr^2[E-e\phi(r)]-J^2\right]^{1/2}} +$$

$$\int_{e\phi(r_w)}^{E_{max}} dE \int_{\sqrt{2m}\, r_w(E-e\phi(r_w))^{1/2}}^{\sqrt{2m}\, r(E-e\phi(r))^{1/2}} dJ \frac{f(E,J)}{m\left[2mr^2[E-e\phi(r)] - J^2\right]^{1/2}}$$

where $E_{max} = \dfrac{r_w^2\, e\phi(r_w) - r^2\, e\phi(r)}{r_w^2 - r^2}$

Assuming f is independent of J.

$$n_e(r) = \int_{e\phi(r)}^{e\phi(r_w)} (\pi/2) dE\, f(E) + \int_{e\phi(r_w)}^{E_{max}} dE f(E) \left\{ (\pi/2) - \sin^{-1}\left[\left(\frac{E-e\phi(r_w)}{E-e\phi(r)}\right)^{1/2} \frac{r_w}{r}\right] \right\}$$

and further assuming a source which is producing a Maxwellian distribution I_1 becomes:

$$I_1 = n_o e^{-e\phi(r)/T_e} \frac{1 - e^{-(e\phi(r_w) - e\phi(r))/T_e}}{1 - e^{-e\phi(r_w)/T_e}}$$

This is just what is obtained when a truncated Maxwellian is integrated over velocity space. I_2 can be evaluated explicitly

if we assume $f \sim 1/E^2$. This is a reasonable approximation because the integral is evaluated over a finite region in E.

$$I_2 = n_o \frac{[e\phi(r_w) - e\phi(r)]}{T_e \left(e^{e\phi(r_w)/T_e} - 1\right)} \frac{\phi(r_w)}{\phi(r)} \left[\left(1 + \frac{r^2\,\phi(r)}{r_w^2\,\phi(r_w) - r^2\,\phi(r)}\right)^{1/2} - 1\right]$$

In evaluating I_2 f has been normalized so that it is equal to the Maxwellian at r_w. With this normalization f will be too big over the range with the largest error coming for larger E where the region of intergration is smaller.

This form of the density goes to zero at the wall and we know that because there is a net electron flux to the wall the density should be finite. It will be finite if we use for the potential at the wall an effective potential slightly larger than that at the wall. This is essentially the result of Pastuhkov[14] who gives for the effective potential,

$$e^{-e\phi_{eff}/T_e} = 3/2\; e^{-e\phi(r_w)/T_e}$$

Using ϕ_{eff} for $\phi(r_w)$, the expression for the density can now be used in Eq. 2.7 in place of the Boltzmann electron term.

Conclusion

In section A we set down three equations, the solution of which determined the electron temperature, density and potential of the plasma created in the neutralizer. We indicated that their solution

could be divided into two separate problems, the particle balance which we examined in Section B, and the energy balance, which we ignored by assuming that the electron temperature was known. In Section B we presented our description of the particle balance. The basic equation was the Tonks and Langmuir plasma sheath equation. Several assumptions were made in its derivation. 1) Electrons are Maxwellian. 2) Ions are born at rest. 3) Ions are accelerated only radially and not axially. 4) The ion beam is the only source of ionization. Assumptions 3 and 4 are supported by experiment. Theory has been developed to eliminate the need for assumptions 1 and 2. The electron density term was modified to include the effects of the potential well and an extra term was added to include ion density caused by ions created with non-zero energy.

The resultant equation has been solved by computer and the results are compared to experimental measurements in Chapter 5.

CHAPTER 3

EXPERIMENT DESIGN

A. Equipment and Procedures

This work was done at Test Stand IIB in the LBL MFE Group. We used a "Berkeley 10-Amp" neutral beam source. The source is described in detail elsewhere[15] but we give a brief description of the system here. The three main sections of the beamline are the plasma arc chamber, the accelerator and the neutralizer. The arc chamber and accelerator mount on the neutralizer which is really nothing more than an aluminum pipe, one meter long and 20 cm diameter, with diagnostic ports installed along its length. This is mounted on a large vacuum tank and the beam is directed into a beam dump. The unit is capable of operating up to 40 keV, 10 amps for 10 ms. The time limit is given by the power supply for the source which is a pulse line. The electronics are indicated in Fig. 5 and the shot firing sequence is also shown. Shots were at one minute intervals. No data were taken during the first 60 shots of any day. This warm-up period was necessary because during this period the operation of the source would change. Runs were made as continuous as possible since any prolonged pause would require several shots to return to the same running condition. Data were reproducible from day to day so long as the proper warm-up was observed. Even so, most data comparisions were made from the same day's data.

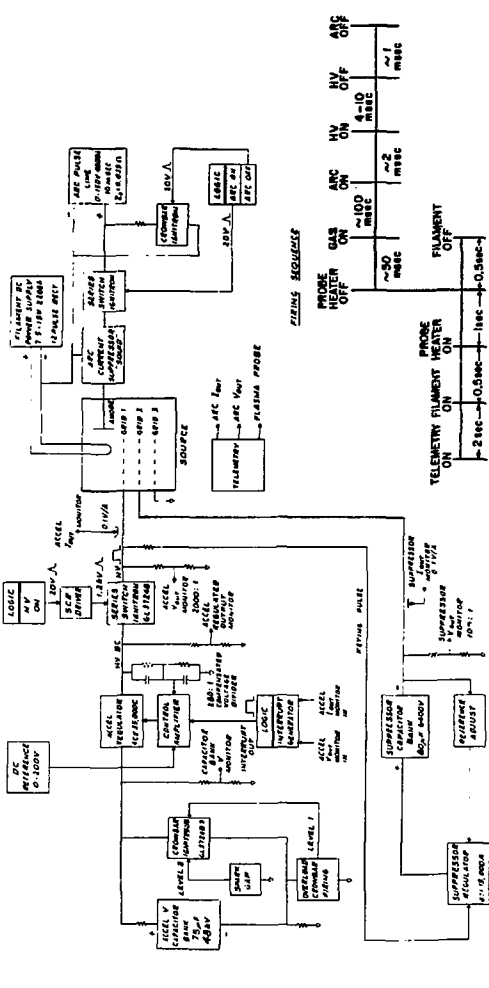
FIRING SEQUENCE
PROBE HEATER OFF
GAS ON
ARC ON
HV ON
HV OFF
ARC OFF
~50 msec
~100 msec
~2 msec
4-10 msec
~1 msec
TELEMETRY ON
FILAMENT HEATER ON
PROBE
FILAMENT OFF
2sec
0.5sec
1sec
0.5sec
SOURCE
PLASMA PROBE
TELEMETRY
FIRING PULSE
XBL824-3762

Figure 5

B. Diagnostics

Several operating parameters are monitored routinely. The source is a hot filament discharge. The discharge current, voltage and saturated ion current are recorded. The accelerator is a three grid structure. The first and last grid provide the potential drop which accelerates the ions. The middle grid is biased negatively to prevent electrons from flowing back into the source from the neutralizer plasma. The operating voltages and currents drawn for these grids are also recorded on an oscilliscope for each shot. The beam profile is monitored at the beam dump which is an array of 32 thermistors imbedded in the aluminum plate. These respond to the heat deposited in the dump by the beam (for more details see Appendix A4). The dump is electrically isolated so that it can be biased relative to ground. The current to the plate is measured by a resistor to ground.

The main data were taken with a 2 mil. diameter tungsten wire which was operated as a Langmuir probe. In addition to getting the electron temperature in the usual way, the probe was used to measure the electron density using the electron collection region in the orbital motion limit.[16] This regime was possible because of the low density present (a few $10^{11}/cm^3$ maximum). Unfortunately, the low density also presented a cleanliness problem. We could not draw sufficient current from the plasma during a shot to clean the probe so the probe had to be cleaned another way. This was accomplished by making the probe a loop of wire and passing a

current sufficient to clean it through the wire before each shot. More details of the contamination are discussed in Appendix A1.

Since the model assumed the plasma flow to be radial, this needed to be tested. Two diagnostics were tried. The first was a planar probe of tungsten which would be rotated about an axis perpendicular to the r-z plane. If the plasma had a component of flow in the z direction one would expect to collect a varying amount over the rotation. Unfortunately, as the normal to the probe points more in the z direction it also begins to intercept more of the 25 keV beam. This is not the main beam which is well collimated, but rather the halo beam which is much less dense and has much more divergence. This halo comes from charge exchange and ionization events that take place in the accelerator. Rather than try to determine the effect of the beam on the probe, another technique was tried.

Ion-acoustic waves travel with the ion-acoustic speed in the local plasma frame. If the plasma is moving with respect to the wave launcher and receiver, the wave speed measured will be the wave speed plus or minus the plasma speed, depending on the direction of the wave propagation relative to the plasma flow. The difference in speeds for a wave launched in opposite direction gives the plasma speed along the line between transmitter and receivers. Doing this along two axes then gives the plasma velocity. (It is really the ion flow velocity but since the ions carry the bulk of the momentum it is essentially the plasma flow.) A probe to make these measurements was designed and is described in Appendix A2.

It is important to know the neutral gas density in order to determine the particle production rates. Two types of ion gauges were used to measure the density. Both used a Varian millitor gauge head but with different electronics to ensure an accurate reading of the density on a short time scale. In its usual operation a sudden puff of gas will cool the filament of the gauge and change the emission of electrons. One type of gauge supply designed at Livermore rapidly regulated the filament current to maintain constant electron emission. The other gauge used the standard supply for the filament and allowed the current to change but it electronically divided the collected ion current by the electron grid current and in this way eliminated the effect of the varying current. Both were calibrated in steady state against a barocel. The gauges agreed with each other, though the Livermore gauge had less ripple owing to its d.c. filament supply. Neither gauge could be relied upon during a shot because the plasma present interfered with the operation of the gauge head. Typical data are shown in Appendix A3.

CHAPTER 4

RESULTS

Most of the data were taken with the thin tungsten wire. It was swept well into both the ion and electron saturation regions. Because of the wire diameter and plasma conditions the probe was in the orbital motion[16] limit of operation. That is,

$$i_{e,i}^2 = \frac{2 A_p^2 n_{e,i}^2 e^2 (e V_b + T_e)}{\pi^2 m_{e,i}}$$

where V_b is the probe bias measured relative to the plasma potential. The ion beam, at 25 keV, is unaffected by the probe bias and adds a term to this equation. It is most noticeable on the probe trace as a shift in the floating potential. In the same way that a hot electron tail lowers the floating point, the ion beam raises the floating potential. In the ion region the beam current will add to the collected current. Also the beam will knock off secondary electrons from the wire which will also add to the current. In the electron region the beam current will reduce the collected current and any secondaries produced will be drawn back to the probe by the probe bias. The transition region will have the proper shape as long as the secondary current is much less than the electron saturation current, that is, it does not act like an emissive probe.

Analysis of a probe trace is a several step process. First the linear extrapolation of the ion current is subtracted off thetrace. Then the plasma potential is determined from the point where

$\frac{\partial^2 I}{\partial V^2} = 0$ (Fig. 6b). This point seems best for a low density plasma where the knee of the trace is not very sharp. What is really important is that a consistent and reproducible definition be used and this method eliminates the somewhat arbitrary choices, such as which intersecting lines to use, from the determination of the potential. The derivatives are taken by Fourier transform on the computer. High frequencies are numerically filtered out in the process. The electron temperature is determined in the usual way from the region below the plasma potential. (Fig. 6c)

The density is obtained from the total current. A two parameter fit is made to the current in the ion region using the equation

$$i = \frac{\sqrt{2}\, A_p\, n_i e}{\pi \sqrt{m_i}} (e(V_p - V_b) + T_e)^{1/2} + I_{b+s}$$

(Here collected ion current is defined to be positive current). V_p and T_e are provided and n_i and I_{b+s} are determined from the fit (Fig. 6d). Because the fit region is far ($>3T_e$) from V_p, n and I are not very sensitive to the value of $T_e + eV_p$. A change of one volt has no effect. Using the secondary emission coefficient for clean tungsten $I_{beam + secondaries}$ is converted to I_{beam}. This is used with the electron region to make a two parameter fit

$$i = \frac{\sqrt{2}\, A_p\, n_e\, e}{\pi \sqrt{m_e}} (e(V_b - V_p) + T_e)^{1/2} - I_b$$

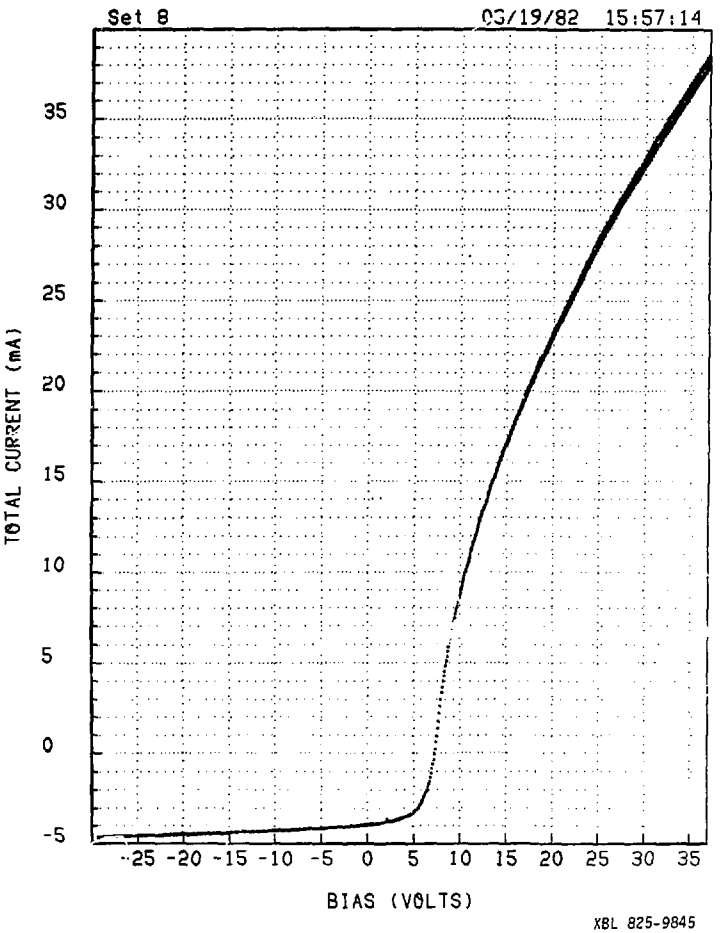
Set 8
03/19/82 15:57:14
TOTAL CURRENT (mA)
35
30
25
20
15
10
5
0
-5
-25 -20 -15 -10 -5 0 5 10 15 20 25 30 35
BIAS (VOLTS)
XBL 825-9845

Figure 6a

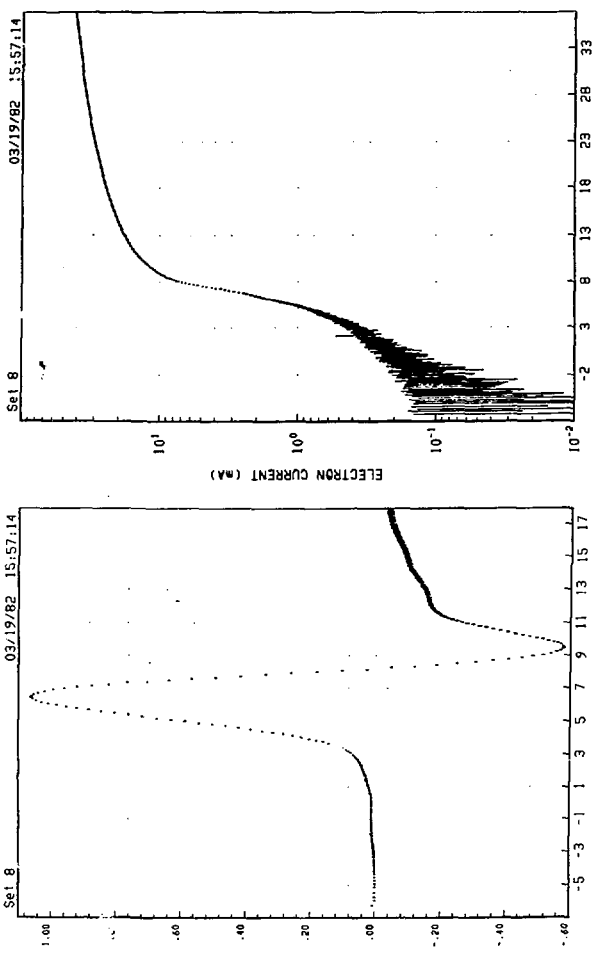

Figure 6b

XBL 825-9839

Figure 6c

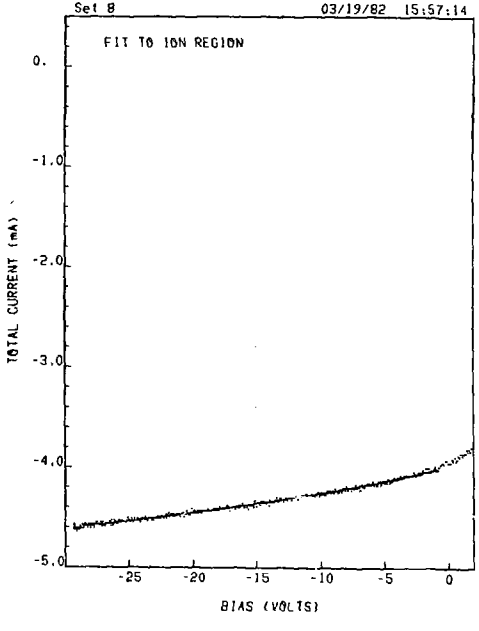

Figure 6d

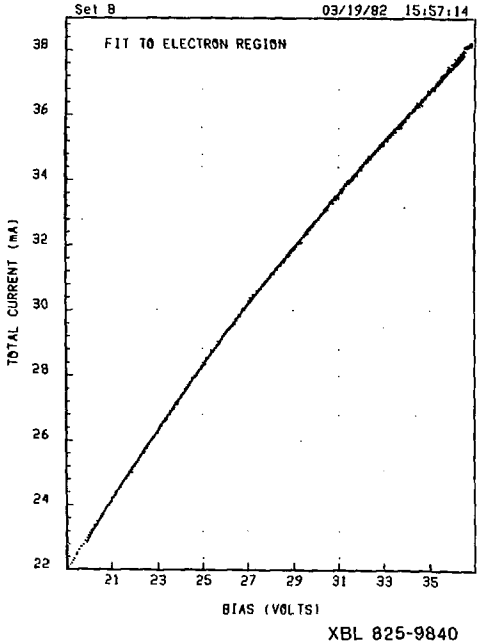

XBL 825-9840

Figure 6e

(Now collected electron current is defined to be positive current and I_b changes sign). V_b is again much greater than V_p ($3T_e$) and $i_p > I_b$ so that I_b is not of great importance. $V_p - T_e$ is not well determined from this method. n_e is then taken to be the density of the plasma (Fig. 6e). I_b gives a measure of the beam current.

There are a large number of parameters that could be varied in this system. Rather than try to cover the entire parameter space we have taken data along the axes of the space to get an idea of what is important and then expanded the coverage in those areas. The first concern is how constant the plasma parameters are during the 10 ms of the shot. We varied the start of the probe sweep by one millisecond intervals through the length of the shot. As seen in Fig. 7a,b the temperature is constant but the density rises during the shot. The change is slow enough that it will not effect the interpretation of a probe trace. We also expect data taken during the same time intervals to be comparable.

The main data consist of the density profiles. The probe could be moved radially without disturbing the system running. The mover had six centimeters of travel and a relative accuracy of better than one quarter of a millimeter. Because the travel was less than the diameter of the neutralizer it had to be set to cover different parts of the beam and one continuous sweep of the entire diameter was not possible. Most of the data were taken from the center out to six centimeters which is approximately two beam radii. Figure 8 shows six profiles taken for three different beam currents at two

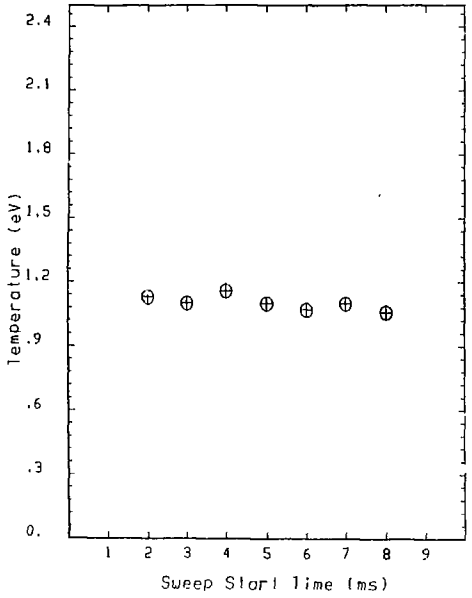

Figure 7a

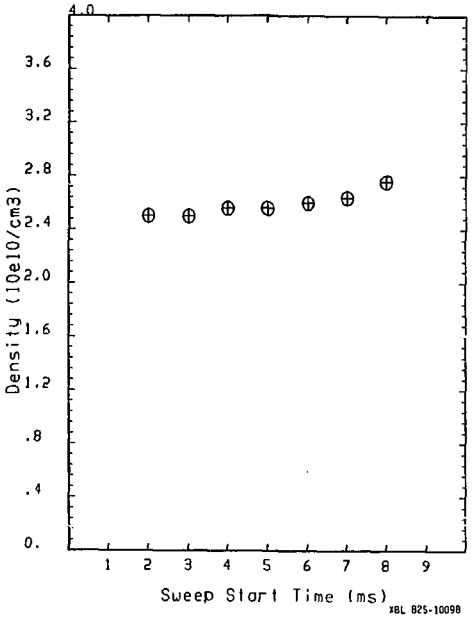

Figure 7b

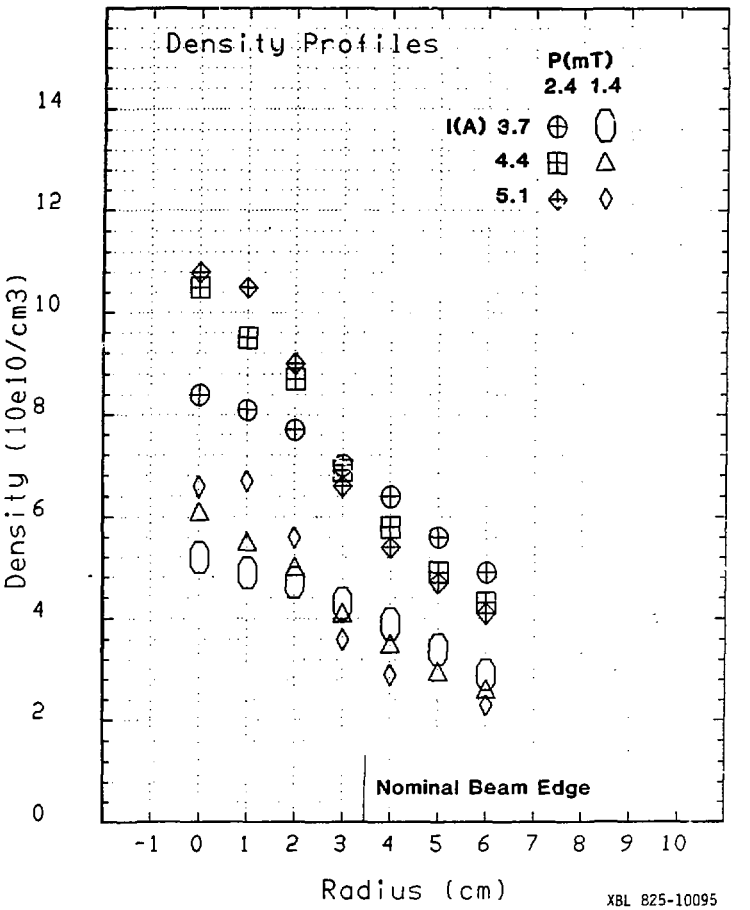
Density Profiles
P(mT)
2.4 1.4
I(A) 3.7
4.4
5.1
Nominal Beam Edge
Density (10e10/cm3)
Radius (cm)
0
2
4
6
8
10
12
14
-1
0
1
2
3
4
5
6
7
8
9
10
XBL 825-10095

Figure 8a

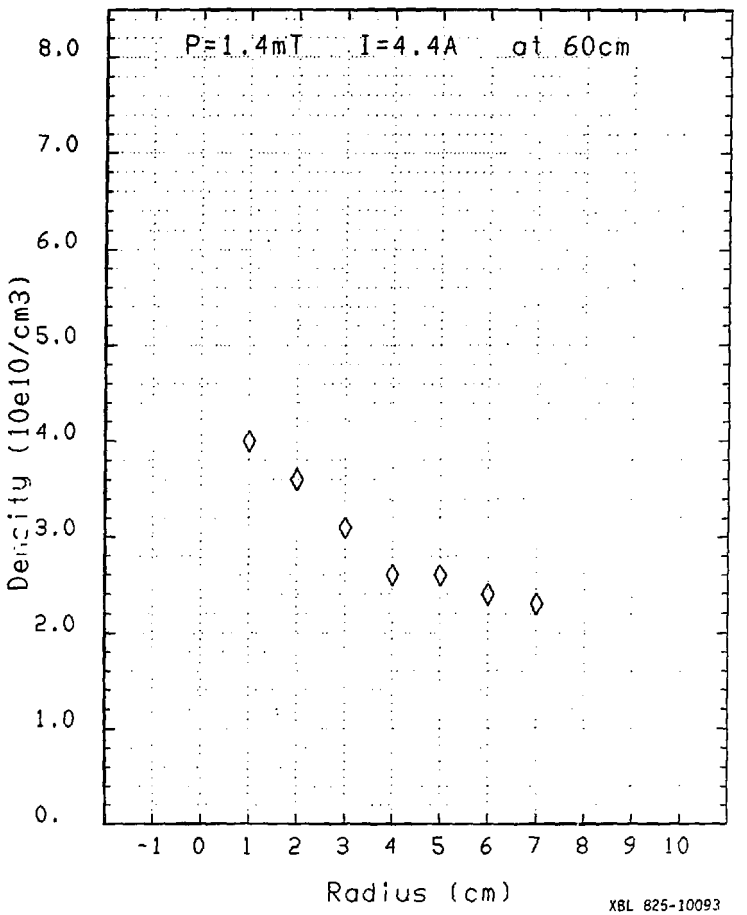
P=1.4mT I=4.4A at 60cm
8.0
7.0
6.0
5.0
4.0
3.0
2.0
1.0
0.
Density (10e10/cm3)
-1 0 1 2 3 4 5 6 7 8 9 10
Radius (cm)
XBL 825-10093

Figure 8b

different neutral gas pressures 30 cm downstream from the exit grid. A small amount of data was also taken 60cm downstream (Fig. 8b). We see from the density plots that the density behaves as expected in the center. It rises with both gas pressure and beam current. At the edge, however, the qualitative behavior with respect to current is the reverse of what is expected. This is due to combined effects of temperature change and divergence change as are discussed in the next section. In addition to the density profiles the data analysis yields plasma potential and beam current profiles (Fig. 9,10). The most surprising result is the variation of the electron temperature with beam current (Fig. 11). The temperature rises by a factor of two while the beam current, and hence the power in, only increases by 50%. The temperature is nearly uniform across the neutralizer showing a slight (.1eV) increase in the region where the beam is present.

The calorimeter/beam dump could be electrically isolated from ground. Since most of the fast electrons are created in the forward direction they strike the beam dump. By putting a bias on the dump we expected to change the fraction of fast electrons, that is, make an increasing number of them part of the slow electron population. When this was done, the density profiles did not change but Fig. 12 shows how the plasma potential changed with bias on the dump.

The ion acoustic probe (Appendix A2) was oriented with normal of the transmitter and receiver parallel to the axis of the beam line in order to measure any unexpected axial flow. The propagation velocity was measured for a wave traveling toward the source and

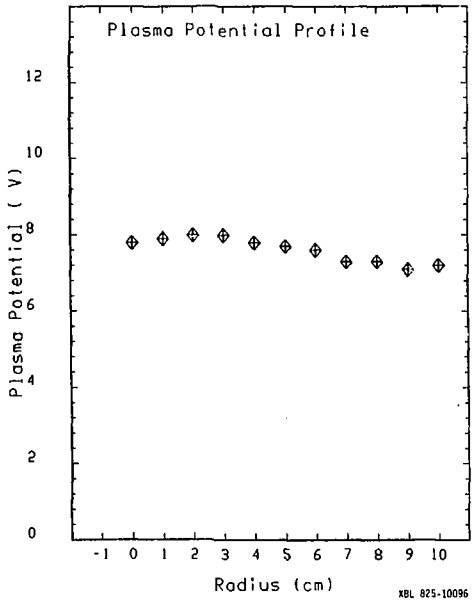
Plasma Potential Profile
Plasma Potential (V)
0
2
4
6
8
10
12
-1 0 1 2 3 4 5 6 7 8 9 10
Radius (cm)
XBL 825-10096

Figure 9

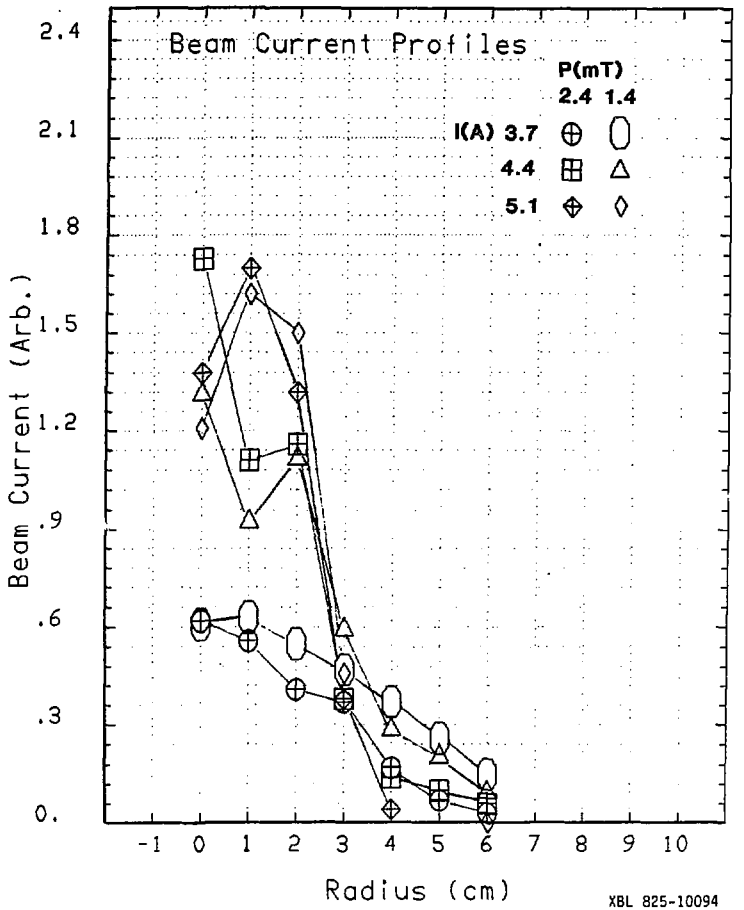
Beam Current Profiles
P(mT)
2.4 1.4
I(A) 3.7
4.4
5.1
Beam Current (Arb.)
2.4
2.1
1.8
1.5
1.2
.9
.6
.3
0.
-1 0 1 2 3 4 5 6 7 8 9 10
Radius (cm)
XBL 825-10094

Figure 10

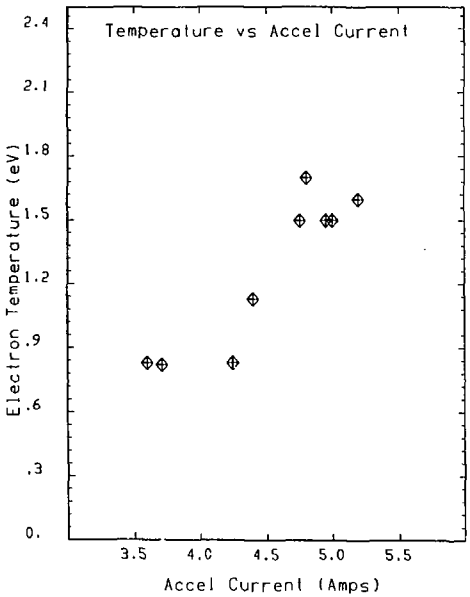

Figure 11

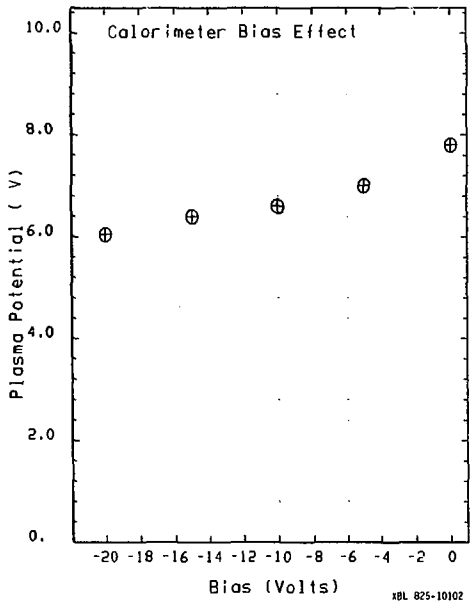

Figure 12

then the entire probe assembly was rotated 180° to measure the downstream velocity. The difference of the two velocities gives the axial flow velocity. This was found to be .1 cm/sec which is on the order of the thermal velocity of the neutral gas. We conclude from this that there is no anomalous axial flow.

CHAPTER 5

DISCUSSION AND CONCLUSION

Discussion

It is the purpose of this research to establish the particle sources and sinks in the neutralizer with the help of Langmuir probes. Toward that end we have measured radial density profiles. Because of the operating conditions the density could be determined from the slope of the characteristic which is more accurate than the methods that determine the density from a single point. These profiles are compared to a model which requires as input measurements of the electron temperature, the neutral gas density, and the ion beam shape, intensity and composition. The temperature was obtained from the transition region in the usual way. The gas density, while it could not be measured during a shot, was bracketed by a cold-gas measurement without a shot and the maximum change that could occur given the geometry of the neutralizer (see Appendix A3). The ion beam profile was measured in two ways, from the calorimeter at the end of the beam line and from the shift in the probe traces.

Before we compare the measured profiles with the computed ones, let us consider where the uncertainties are. Langmuir probes are accurate devices for measuring the temperature, but it is always difficult to get an absolute measure of the density from them. Though the theory is quite good in the orbital motion limit there are several systematic effects that limit accuracy. The probe is

not an infinite cylinder, it is curved into the shape of a loop and has ends. There are uncertainties in the probe area and in the reading resistor. Because of these, we will take the error to be around 20 percent. This is probably optimistic. The relative uncertainty, however, is probably much better. Only the plasma density and the amount of support structure change as the probe position is varied. The support structure probably causes the decline in plasma potential measured in the center. The variation in the density is not great and produces a small change in the Debye length which governs the accuracy of the theory.

The largest uncertainty is in the beam profiles. That part of the beam which is well collimated is accurately represented by the calorimeter data. The widely divergent part of the beam, the halo, will not arrive at the calorimeter to be recorded. The probe indicates wings on the beam wider than that given by the calorimeter. But at the edge where the beam amplitude is small, the error in the measurement is comparable to the magnitude of the beam current. Measurements on other beam lines have indicated a nearly constant amplitude halo beam extending all the way to the wall.[17] This halo is also seen to be insensitive to beam tuning. To account for this in the model we have added to the beam shape a small amplitude (15 percent) gaussian with five times the divergence of the main beam. This was chosen to fit the wing of the beam profile for the 4.4 Ampere case.

In generating the computer profiles the temperature, on axis plasma density, beam current at the exit grid and shape factor are

inputs. The ion generation rate is then adjusted until the sheath and the real wall location coincide. That ion generation rate can then be compared with the rate determined from the measured gas density. Figures 13abcdefg show the curves and data for the six cases shown in the results section. Figure 14 shows another case where the measurements were extended to the wall. Figure 15 is the same case as Fig. 6 but without the halo added to the beam. Note that the halo is needed to produce the density measured outside the beam edge. The calculated generation rates are within 20 percent at the expected rates (see table) which is quite good considering the absolute uncertainty in the density.

Pressure (mT)	1.4			2.4		
Beam Current (A)	3.7	4.9	5.1	3.7	4.4	5.1
Calculated Rate	.63	.94	1.2	.95	1.4	1.7
Expected Rate (10^{16} cm^{-3}/sec)	.74	.88	1.0	1.1	1.4	1.6

The general agreement of the computed and measured profiles and the agreement of the production rates gives us confidence that we have identified and correctly assesed the magnitude of the particle source and that we understand where the particles go. Also on the time scale of this experiment we see no evidence that the gas density in the neutralizer is other than that expected from molecular gas flow. On the other hand, there is no obvious explanation of the electron temperature variation observed. We hope that the work presented here will supply a solid foundation for examining the problem.

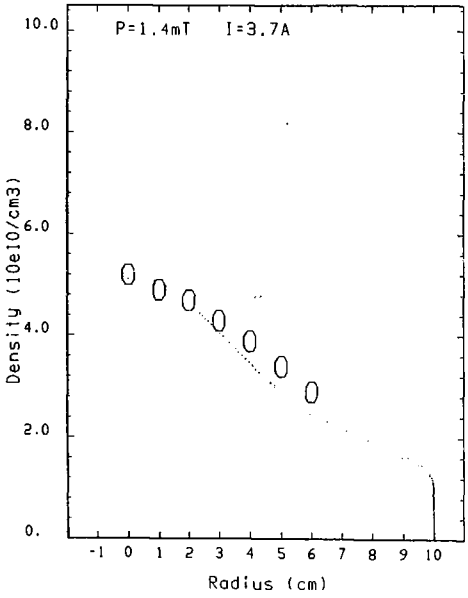

Figure 13a

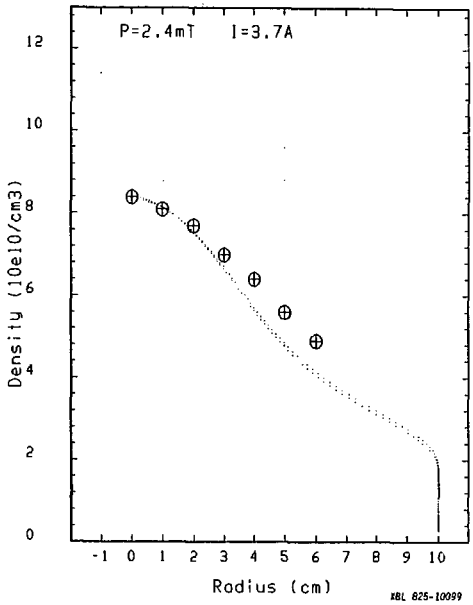

Figure 13b

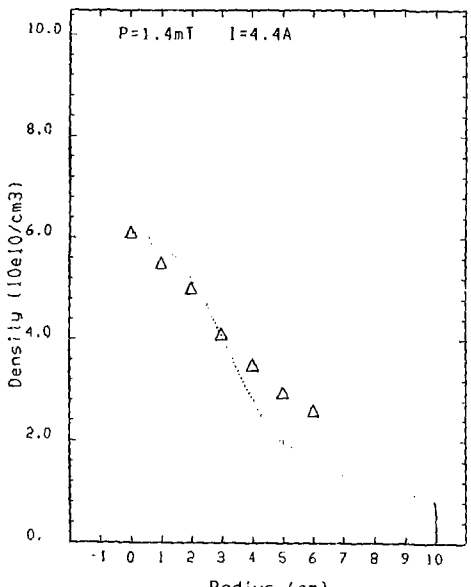

Figure 13c

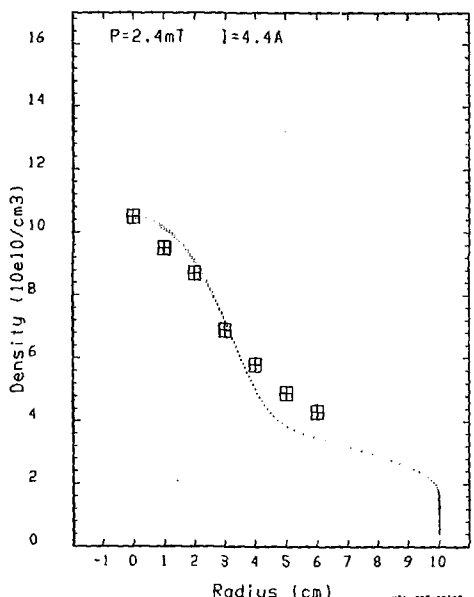

Figure 13d

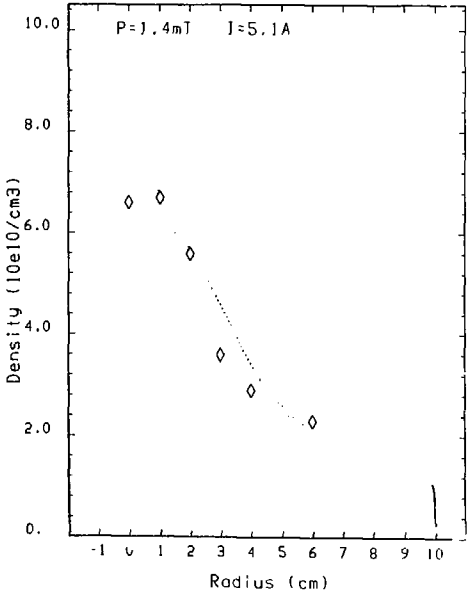

Figure 13e

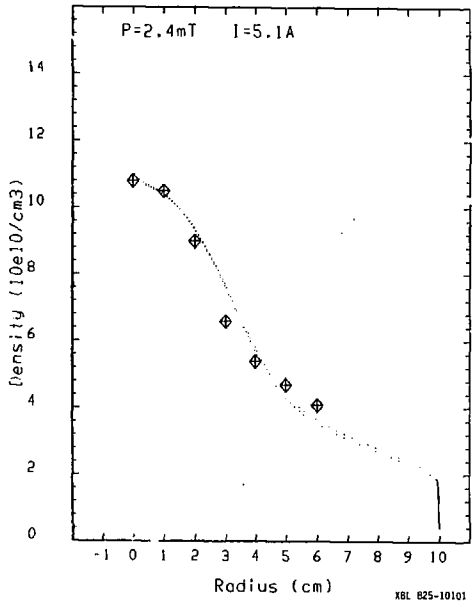

Figure 13f

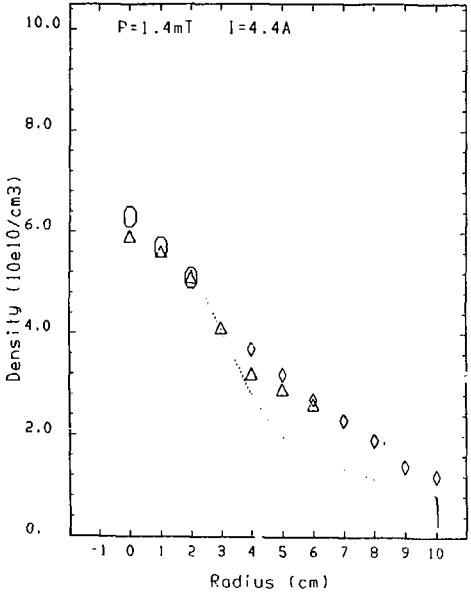

Figure 14

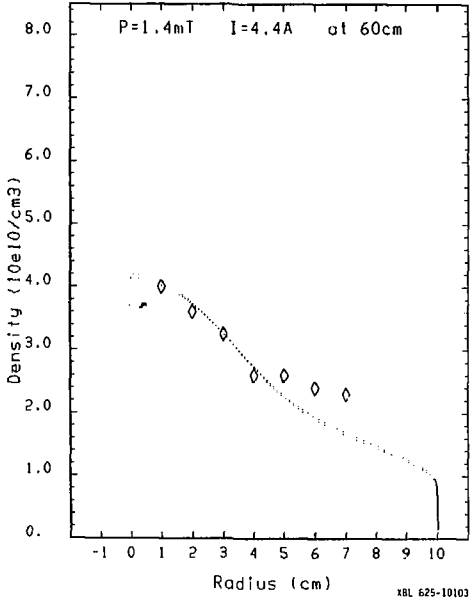

Figure 13g

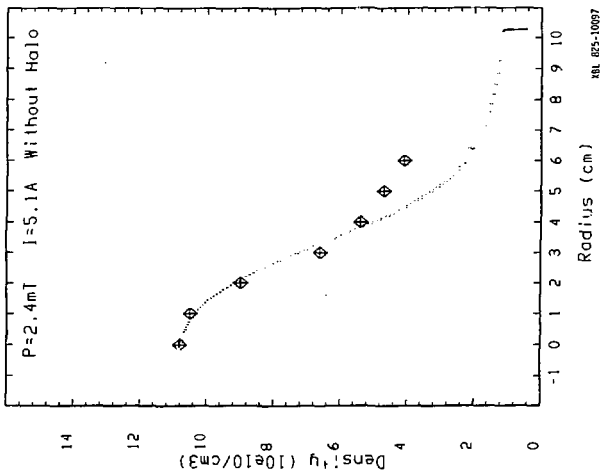
P=2.4mT I=5.1A Without Halo
Density (10e10/cm3)
0
2
4
6
8
10
12
14
-1 0 1 2 3 4 5 6 7 8 9 10
Radius (cm)
KBL 025-10097

Figure 15

Though it was not mentioned specifically in Chapter 2 the model for the neutralizer plasma does not require local ambipolar flow. In the steady state the ion and electron loss rates are equal, but some of the electrons are lost axially to the beam dump while all of the ions are lost radially to the walls. Biasing the beam dump negative will prevent electrons from being collected there and force them to go to the walls. As indicated by Eq. 2.2 reducing the fraction, f, of electrons that leave via the end will reduce the plasma potential. Without a detailed knowledge of space and energy distribution of the newly created electrons, it is impossible to determine f. But qualitatively one expects the change in plasma potential to saturate for large bias. The measured shift in plasma potential with varying beam bias supports this picture. Other possible effects of the bias such as introducing several amperes of cold electrons, would effect the electron temperature or the density profiles, neither of which change when the bias is applied. There may be other unknown processes so this is not a proof but it is strongly suggestive.

Conclusion

We have presented a model for the neutralizer plasma in which we follow the production and loss of individual ions and electrons . The electrons are born with a spread in energy, some of which will escape the potential well immediately and others that will be trapped and require some scattering in order to escape. The ions, whether created by charge exchange or by ionization, will accelerate

radially to the walls. The steady state is established by the plasma potential adjusting itself so that the loss rate for the trapped electrons is correct. Most of the energy comes from the energy the electrons receive when they are created. As the fast electron goes to the wall it gives to the potential well exactly the energy that an ion born along with the electron will remove when it goes to the wall. The only extra energy needed in the system is that amount by which the slow electrons are trapped. The source of this energy has not yet been identified.

We have patterned a model for the radial ion flux after the Tonks-Langmuir plasma sheath equation We have replaced the ionization by electrons with ionization by an ion beam. We have also included effects of the truncated electron distribution, and the effect of having some of the ions born with initial energy. The solution of the resulting equation by computer confirms our understanding.

The experimental findings, as far as the ion beam and the state of the neutralizer is concerned, can be summarized as follows: The neutralizers for large intense ion beams contain plasma generated primarily by the beam. The density of this plasma exceeds that of the beam by at least one order of magnitude. This was expected and had been seen before. On the other hand, the ion beam density distributions that we observed here were a surprise. They were surprising because they disagreed with the calorimetry data. In addition to the structure near the axis, the beam had a much larger than expected halo. Though the beam measurement had a large

uncertainty in the halo region the density measurement and the computer profiles indicated that the large halo was real. We had noadditional diagnostic to confirm the detail in the center of the beam but the result was reproducible at different pressures and at different positions along the neutralizer. This effect may be due to the arc discharge operation, i.e., nonuniformities in the source, and while it does not invalidate this experiment it is of concern to neutral beam source developers.

The temperature variation with ion beam current was also unexpected. Evidently, the energy balance for electrons is complex. The matter is of considerable interest and will be the topic of future research at this test stand.

The measured density profiles we believe accurately establish the plasma shape in the neutralizer and will be useful in the future energy balance research and in the interpretation of neutral beam behavior in other injection systems.

REFERENCES

1. Cooper, William S., Lawrence Berkeley Laboratory, Private Communication.
2. Holmes A. J. T., Culham, Private Communication.
3. Tonks, L. and Langmuir, I., Physical Review 34, 4 (1929).
4. Parker, J. V., Physics of Fluids, 6, 1658 (1963).
5. Dunn, D. A., and Self, S. A., Journal of Applied Physics. 35, 113 (1964).
6. Self, S. A., Journal of applied Physics, 36, 456 (1965).
7. Kino, G. S., and Shaw, E. K., Physics of Fluids, 9, 587 (1966).
8. Hooper, E. B., Anderson, O. A., and Willman, P. A., Physics of Fluids 22, 2334 (1979).
9. Gabovich, M. D., Katsubo, L. P. Soloshenko, I. A., Soviet Journal of Plasma Physics, 1, 162 (1975).
10. Holmes, A. J. T., Phys. Rev. A 19, 387 (1979).
11. Kuyatt, C. E. and Jorgensen, Jr., T., Physical Review, 130, 1444, (1963).
12. Barnett. C. F., Ray, J. A., Ricci, E., Wilker, M. I., McDaniel, E. W., Thomas, E. W., and Gilbody, H. B., ORNL-5207 and 5207.
13. Bernstein, I. B. and Rabinowitz, I. N, Physics of Fluids 2, 112 (1959).
14. Pastukhov, V. P. Nuclear Fusion 14, 3 (1974).
15. Ehlers, K. W., Baker, W. R. Berkner, K. N., Cooper, W. S., Kunkel, E. B., Pyle, R. V. and J. W. Stearns, J. Vac. Sci. Technol. 10, 922 (1973)

16. Langmuir, I. and Mott-Smith, H. M. (Gen. Elec. Rev. 27, 449 (1924). Goodall C. V. and Polychronopulos B., Planet. Space Sci. 22, 1585 (1974).

17. Vella, M. C. and Willis, J., A Radiatively Driven Beam Power Probe, Lawrence Berkeley Laboratory Report No 14379.

18. Rehmann, Wilhelm K. and Stone, Nobie H., AIAA J. Tech. Notes 8, 1717 (1970).

19. Wong, A. Y, Motley, R. W., and D'Angelo, N, Phys. Rev. 133, A436 (1964).

20. Alexeff, I., Jones, W. D., Lonngren, Karl, Montgomery, David, Phys. Fluids 12, 345 (1969).

21. Christensen, Thomas and Hershkovitz, Noah, Phys. Lett. A 61, 170 (1977).

22. Joyce, Glen, Lonngren, Karl, I. and Jones, W. D. Phys. Fluids 12, 2592 (1969).

23. Chan, Chun-Fai, Lawrence Berkeley Laboratory, Private communication.

24. Bohm, D. Characteristics of Electrical Discharges in Magnetic Fields, edited by A. Guthrie and R. K. Wakerling, McGraw Hill, New York, Chap. 3 (1949).

25. Hiskes, J. R., Karo, A. M., Bacal, M., Bruneteau, A. M. and Graham, W. G., Hydrogen Vibrational Population Distributions and Negative Ion Concentrations in a Medium Density Hydrogen Discharge, UCRL 86873 (1981).

APPENDIX A1

Electrostatic Probe

A serious problem with the use of probes in this plasma was surface contamination. Figure 16a shows three probe sweeps of overlapping voltage ranges. Where the voltage is the same the current drawn should be the same. This was not the case and in fact for one range the current actually decreased. This indicated the need to clean the surface of the probe. Figure 16b shows the same plasma conditions, but after cleaning. Here the traces can be seen to behave correctly. To understand the effect of the contamination, we tried to simulate a "dirty" probe by putting a capacitor in series between the probe and the supply. The result is shown in Fig. 16c. The contamination was probably forming a thin insulating layer on the probe surface causing it to act like the capacitor.

The probe was designed with the need to clean it in mind. Because of the low density and short duration of the plasma under investigation, the plasma current could not be used to clean the probe. The probe was made of a loop of tungsten wire, 2.5 cm long x 2 mil diameter. The tungsten was spot-welded to larger steel wire. The steel wire passed through two holed alumina held inside 1/4" copper tubing. The welds were recessed into the insulator so that only the tungsten would contact the plasma and collect current. A separate d.c. power supply provided the current to heat the probe. Measurement by optical pyrometer indicated a probe temperature of 2100°C when heated. Circuitry was arranged so that the time between

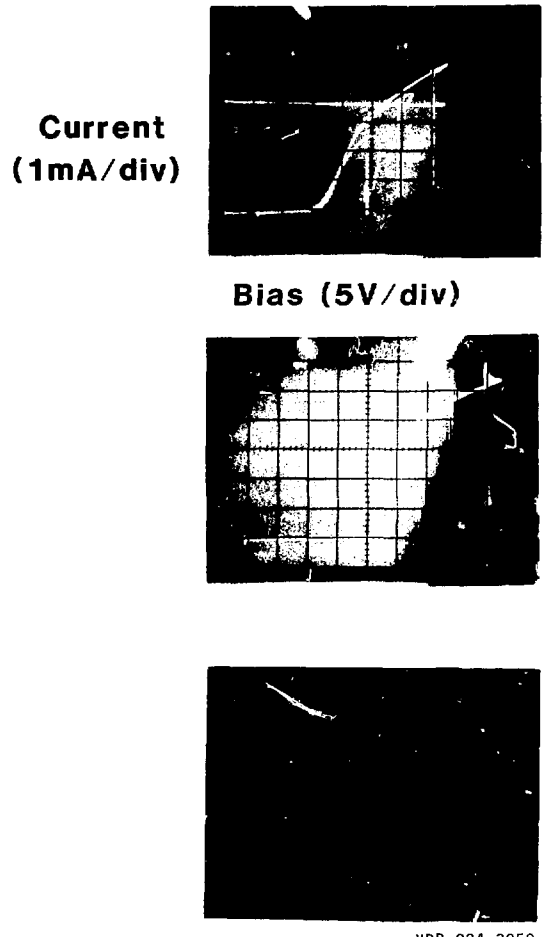

Figure 16

the heating and the shot could be varied. A second level of contamination was found. The problem shown in Fig. 16 would re-occur after about a week, if the probe was not cleaned during that time. But this second level occurred in less than one second. Figure 17 compares two traces, one taken immediately after cleaning and the other with the cleaning advanced to one second before shot. The later trace appears to have been shifted one volt positive. Because of this we tried to heat the probe as close to the shot as possible. We could also get too close to the shot because of the ion beam. By itself the ion beam striking the probe did not heat it enough to have an effect, but when the probe was heated too close to the shot, the energy from the beam, plus the heat that had not dissipated yet was enough to make the probe emissive. We settled on heating for 1.5 seconds ending 100 ms before the shot and when an emissive prove was wanted, it was heated with a higher current ending 2 ms before the shot.

Figure 18 shows the probe circuitry. The heating supply was switched in and out by a mechanical relay on both legs to ensure that during the shot the supply presented neither a large capacitor nor an additional path to ground. The probe sweep was provided by a capacitor (C1) discharging through an inductor (L1). The capacitor would be charged back up again between shots by the battery (B1). In this way, the reading resistor presented the only path to ground for the current drawn by the plasma. The probe current was then

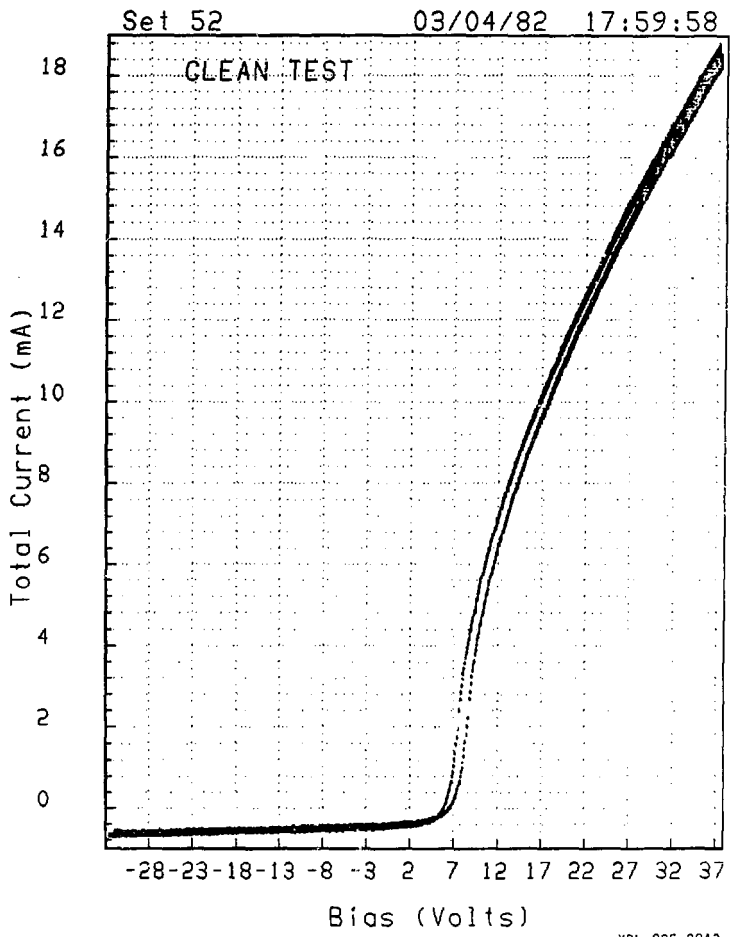
Set 52
03/04/82 17:59:58
CLEAN TEST
Total Current (mA)
0
2
4
6
8
10
12
14
16
18
-28 -23 -18 -13 -8 -3 2 7 12 17 22 27 32 37
Bias (Volts)
XBL 825-9843

Figure 17

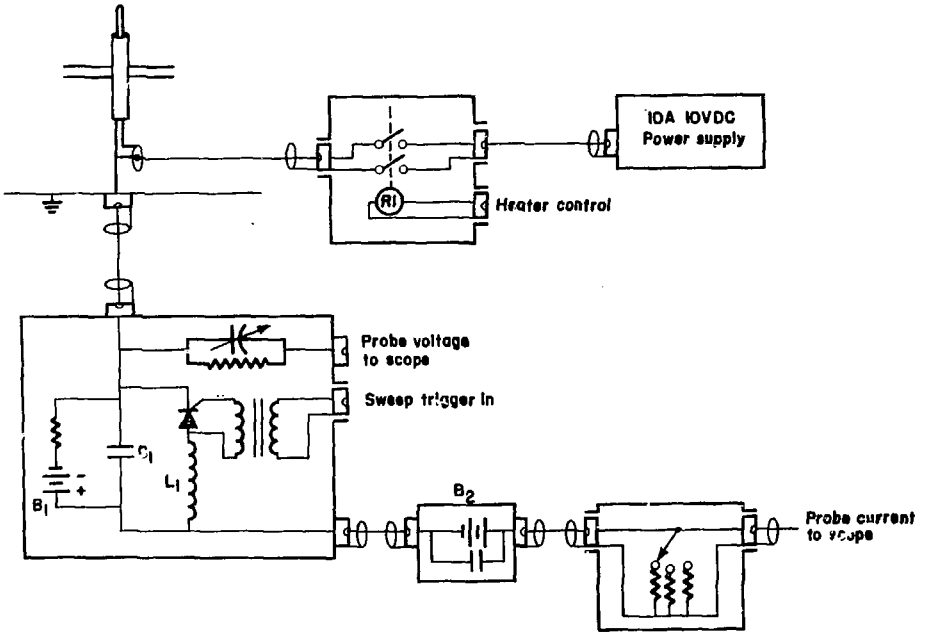

Figure 18

XBL 823-300

monitored by measuring the voltage on that resistor. The probe voltage was monitored by a high impedance voltage divider using the scope input as part of the divider. The voltage is measured at the probe so that even if the capacitor voltage was pulled down by the current drawn by the plasma (as is the case in the far electron saturation region) or the current through the reading resistor produced a significant voltage shift, the correct value is recorded. The trim capacitor compensated for the cable and input capacitance of the scope to ensure accurate readings during fast sweeps.

Probe voltage and current were recorded as a function of time on a Nicolet transient digitizer. A current baseline with no plasma present was also recorded. These were transferred to a computer where the baseline was subtracted off. The sweep (2 ms) was kept slow compared to the ion plasma period, typically $\partial V/\partial t = 3 \cdot 10^4$ Volts/sec $\ll T_e \cdot \omega_{pi} = 1.5 \cdot 10^7$ Volts/sec, so that the probe characteristic could be considered quasistatic.

APPENDIX A2

Ion Acoustic Probe

In order to detect any axial flow of the plasma in the neutralizer this ion-acoustic diagnostic was developed. The plan was simply to launch waves from one grid and receive them at another, and then measure the time of flight of the wave.[18] This was to be done in several directions so that the velocity vector could be obtained from its components. It did not work because direct coupling and power supply ripple at an unfortunate frequency made it too difficult to obtain a good signal. Phase sensitive techniques which vary the probe separation and observe the signal going in and out of phase[19] also could not be used because the plasma is pulsed for such a short time with such a slow repetition-rate. The method we developed circumvents these problems.

Waves are sent with a time varying frequency. The difference frequency between the transmitted and received signals resulting from the change in transmitted frequency during the transit time is observed. If the frequency is swept linearly in time, the difference frequency will be constant and proportional to the transit time. Let T(t) and R(t) be the transmitted and received signals respectively.

$$T(t) = \sin \phi(t) \tag{1}$$

$$R(t) = \sin \phi(t - \delta t) \tag{2}$$

where $\phi(t)$ is the phase function of the transmitted wave and δt is the transit time. For probe separation s and wave velocity V, $\delta t = s/V$.

These signals are mixed electronically. The resulting signal, M(t) is

$$M(t) = R(t)\ T(t) \tag{3}$$

$$= \sin \phi(t) \sin \phi(t - \delta t) \tag{4}$$

$$= 1/2 \cos [\phi(t) - \phi(t - \delta t)] - 1/2 \cos [\phi(t) + \phi(t - \delta t)] \tag{5}$$

The high frequency component is filtered out, and the signal

$$M'(t) = 1/2 \cos [\phi(t) - \phi(t - \delta t)] \text{ is recorded.} \tag{6}$$

For a linearly varying frequency ramp of the form

$$f(t) = f_0 + (\partial f/\partial t)\ t \tag{7}$$

the phase function will be

$$\phi(t) = \phi_0 + 2\pi f_0 t + \pi (df/dt)\ t^2 \tag{8}$$

Now let

$$\psi = 2\pi f_0 \delta t - \pi (\partial f/\partial t)\ \delta t^2 \tag{9}$$

and

$$F_d = (\partial f/\partial t)\ \delta t \tag{10}$$

then $$M'(t) = 1/2 \cos (\psi + 2\pi F_d t) \tag{11}$$

and the velocity $V = s/\delta t = \frac{s\ \partial f/\partial t}{F_d}$ (12)

Note that noise of a fixed frequency such as the power supply ripple will leave the mixer as a spread of frequencies, and direct (electromagnetic) coupling will produce a dc offset on the signal. The number of periods of the difference frequency, N, depends only on the range of frequency swept and not on the measurement time, t_m

$$N = F_d \cdot t_m = \frac{\delta F}{\delta t} \cdot \delta t . t_m = \frac{F_2 - F_1}{t_m} \cdot \delta t \cdot t_m = (F_2 - F_1) \cdot \delta t \quad (13)$$

There are two constraints on the times involved. (1) Experimentally the frequency can be swept only to some maximum value (F_M) above which a linear wave no longer propagates. Thus to observe at least one period (N = 1) eq. (13) requires that $\delta t > 1/\delta F > 1/F_M$. (2) The change of driver frequency in its period must be small compared to the driver frequency. In particular $\delta f/\delta t\ 1/F_1 << F_1$ which implies $t_m >> \delta t$.
Neither of these is a severe restriction; the practical limit comes from the external circuit elements.

Since the number of periods does not depend on the sweep time, this technique can be conceptualized as analogous to the phase sensitive techniques mentioned earlier. Here it is the wavelength that is varied instead of the probe separation and the output signal goes through a maximum as an integer number of wavelengths matches the probe separation (Fig. 19).

Standard Phase Sensitive Technique Transmits at a Fixed Frequency (f) and Varies the Distance (S) to the Receiver

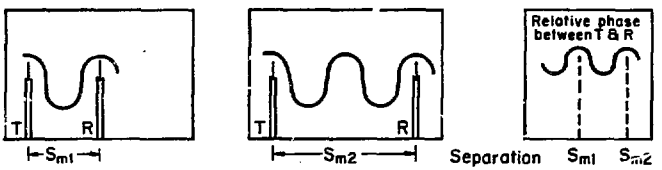

This Technique Maintains a Constant Separation (S) and Varies the *Transmitted Frequency*

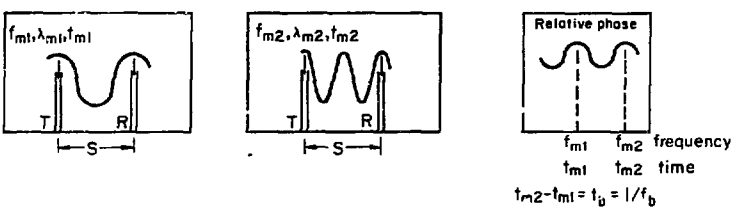

XBL824-3761

Figure 19

The I-A probe consisted of two nearly identical pieces of tungsten mesh (70% transparent, 200 lines per inch) mounted on the ends of coax. The mesh was spot-welded to steel wire which passed through alumina and copper tube to form the coax. The assembly was sealed with epoxy. The two coaxes were bent in doglegs of different lengths. In this way, the separation could be set to four distinct positions by rotating the coaxes. They could also be moved in or back relative to the flange (Fig. 20).

A schematic block diagram of the electronics is shown in Fig. 21. The grids were biased in the ion saturation region. R1 provides ground reference for the bias. C1 and the internal input resistance form a high pass filter to block the steady ion current. R2 and C2 are chosen to ensure that the phase delay around the two legs is identical.

A consideration in determining the velocity is that the wave is not launched from the grid but from a pre-sheath around the grid.[20] Additional complications result if a wave is simultaneously launched from elements which are electromagnetically coupled to the antenna.[21] To test for these effects, measurements were made at several grid separations and the velocity was determined from the slope of a graph of transit time verses separation. Extrapolation to zero transit time showed that the waves came from the transmitter within the accuracy of the extrapolation ($\pm$ 2 mm), hence this source of error was neglected (Fig. 22).

To avoid disturbing the ion flow, fine mesh grids were used to excite the ion-acoustic waves. Such grids can also launch streams

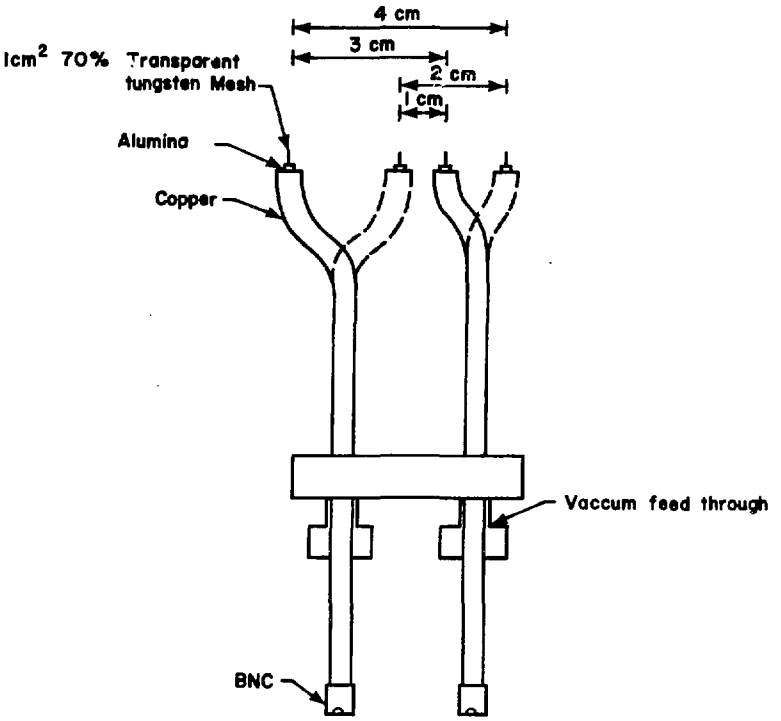
4 cm
3 cm
2 cm
1 cm
1cm² 70% Transparent tungsten Mesh
Alumina
Copper
Vaccum feed through
BNC
XBL 823-299

Figure 20

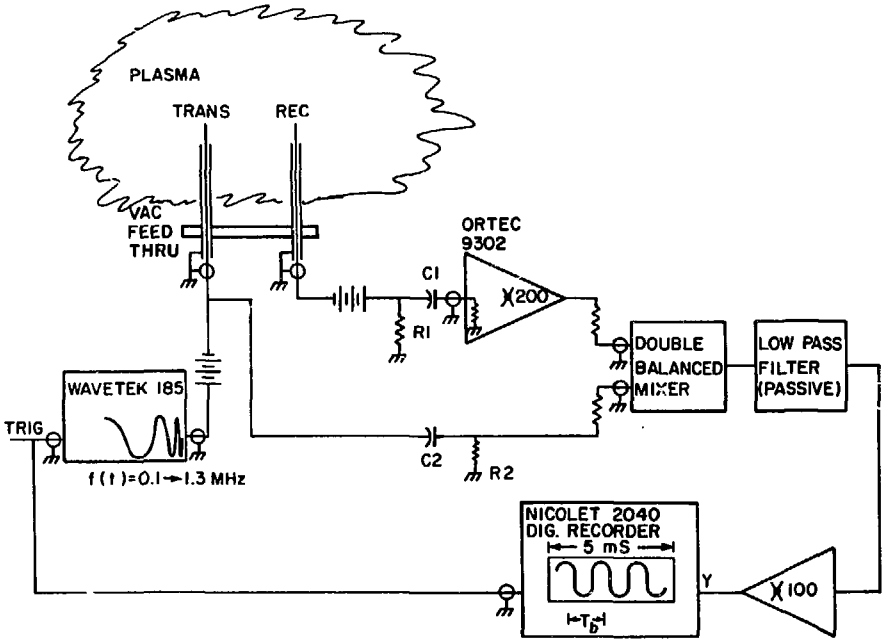

Figure 21

XBL822-4498

Figure 21

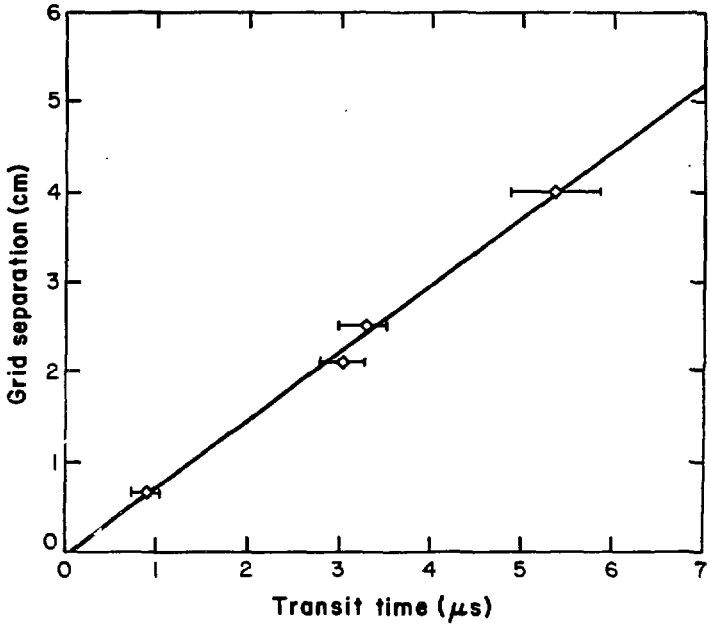

XBL 822-115

Figure 22

of ions known as pseudowaves.[22] Pseudowave speed is a function of the exciter amplitude and frequency. Because of this frequency dependence, the net output would have a changing period, as opposed to the constant period observed. Another check for pseudowaves was done by varying the amplitude by a factor of four. No change in the wave velocity was observable.

A comparison of T_e as measured by a Langmuir probe and as determined by V_{IA} is shown in Fig. 23. The wave was launched in a direction where the effect of flow is minimal and under conditions where T_i and the flow are expected to be small but not zero. The least squares fit for the slope is 1.0 ± 0.3. Given the uncertainties introduced by variations in T_i, flow, and the launch point and the increased signal damping observed for larger T_e, we feel the agreement is reasonable.

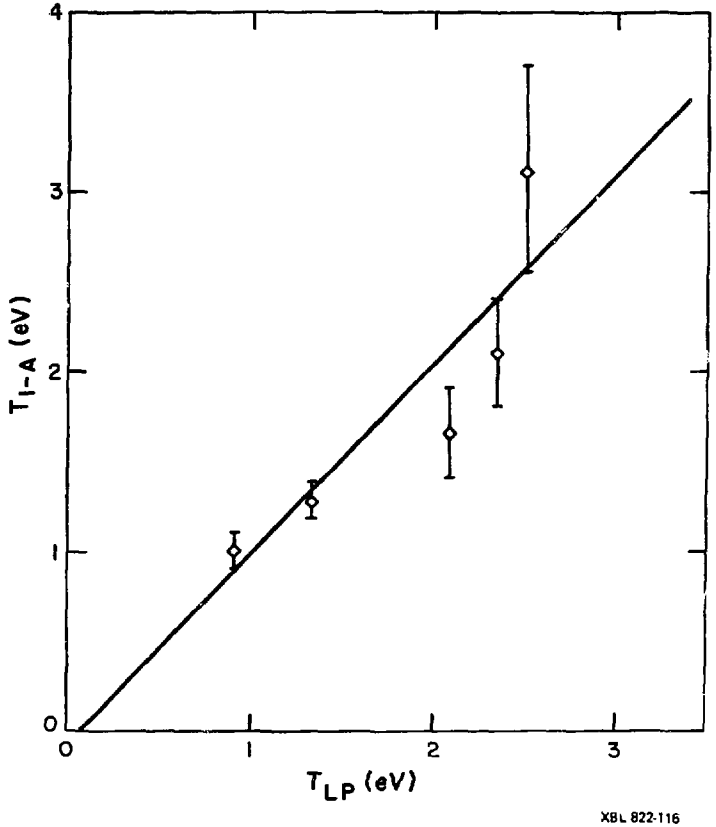

Figure 7

APPENDIX A3

Fast Ion Gauge

The input parameters to the model depend strongly on the neutral gas pressure. It enters the production rate in two ways. First, the production is directly proportional to the neutral density. Second, the composition of the beam, that is, the percent ion and the precent neutral, is a function of the target thickness to that point. This changes the effective cross section for the beam (see Appendix D). It also enters in the same way in the beam ion density at the point of interest. So we would like to know the neutral density as accurately as possible.

Figure 24 shows the output of the ion gauge when no shot is taken and only the gas is turned on. Note the rise time at the start of the pulse. It is ~ 10 ms, which is consistent with the calculated time constant for the neutralizer assuming molecular gas flow.

$$\tau = \frac{\text{Volume}}{\text{Conductance}} = \frac{\pi r^2 L/1000 \text{ liters}}{381\ r^3/L \text{ liters/sec}} = \frac{\pi L^2}{3.8 \cdot 105\ r} \text{ sec} = 8 \text{ ms}$$

The response of the gauge is changed when there is plasma present (Fig. 24). This persists even when the gauge is shielded by a fine mesh. It has been reported that the neutral pressure during a shot is two or three times less than that expected from cold molecular gas flow calculations. This is attributed to the source either heating the neutral gas or causing it to stream preferentially down

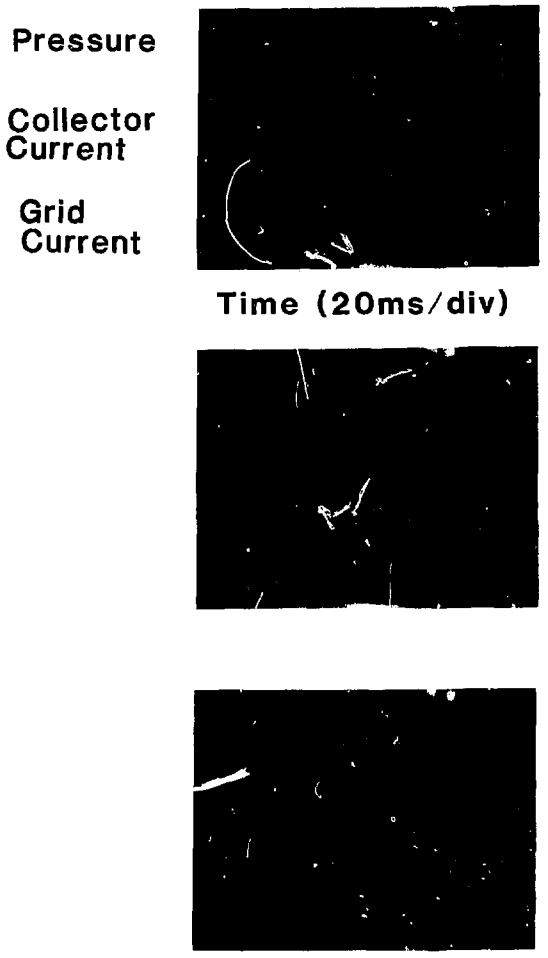
Pressure
Collector Current
Grid Current
a.
Time (20ms/div)
b.
c.
XBB 824-3951

Figure 24

the center of the neutralizer. We do not expect this to be a concern here because the time constant for flow in the neutralizer is longer than the time at which most of the data is taken. Even if new gas is being introduced at a higher temperature it still takes time for the gas present at the start to leave the area.

Appendix A4

Calorimeter

The beam profile is measured at the end of the beam line by the calorimeter. It is a 4 x 8 array of thermistors mounted on an aluminum plate. The thermistors respond to the heat deposited in the plate by the ions and neutrals when they strike the plate. There is no provision on this test stand to deflect the ions and obtain separate profiles for neutrals. The thermistors are monitored by computer and the peak temperature change is recorded for each shot automatically. The center rows and columns are separately fit to gaussians. The fit is done using the curve fitting program PISA. The form chosen is $Ae^{-(\frac{x-x_0}{D})^2}$ where A, the amplitude, X_0, the offset from center, and D, a measure of divergence, are the fit parameters. A sample fit is shown in Fig. 25. Divergences are measured for several values of current to give a tuning curve for a specific accel voltage. Tuning curves at 15, 20, 25, and 30 keV are shown (Figs. 26abcd). The angle is that for the 1/e point of the gaussian.

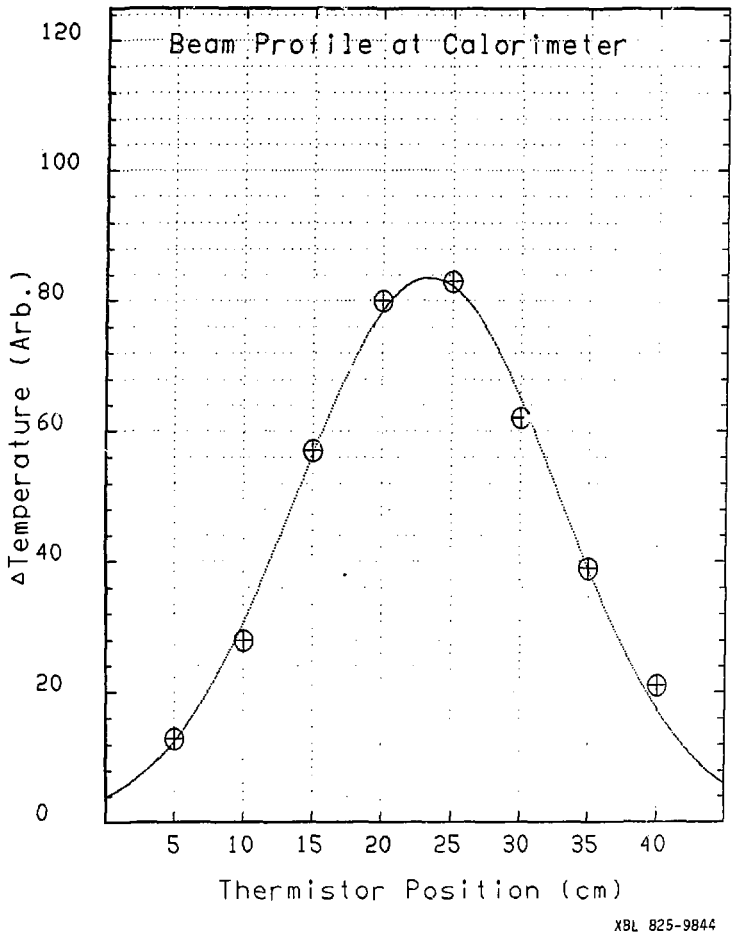
Beam Profile at Calorimeter
120
100
80
60
40
20
0
ΔTemperature (Arb.)
5
10
15
20
25
30
35
40
Thermistor Position (cm)
XBL 825-9844

Figure 25

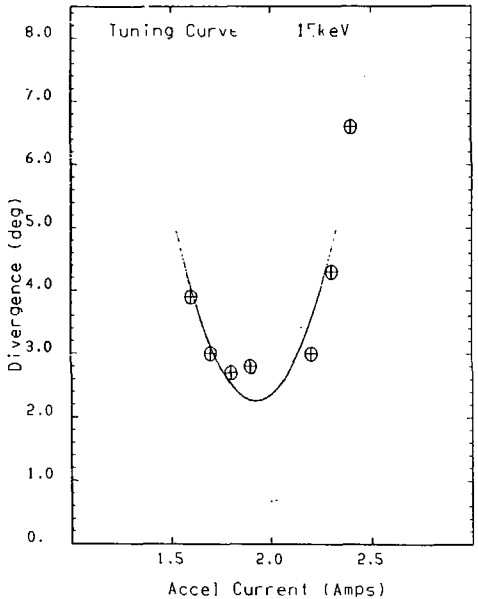

Figure 26a

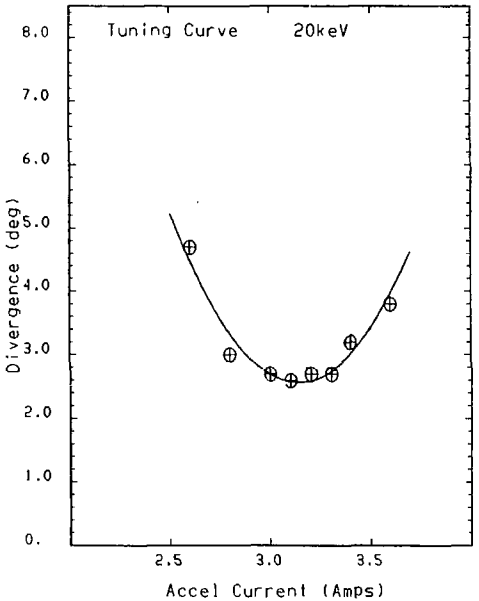

XBL 824-9351

Figure 26b

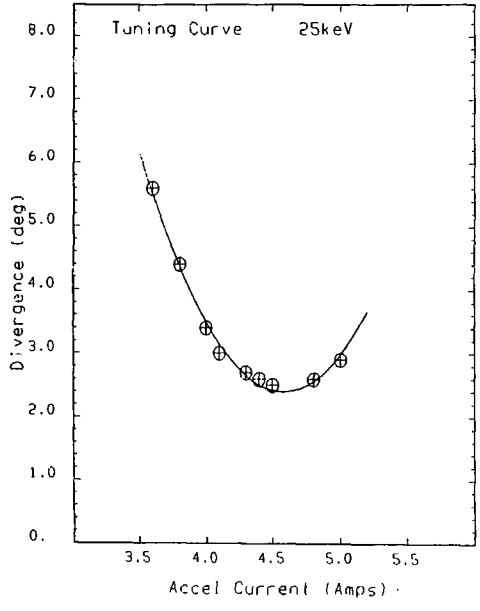

Figure 26c

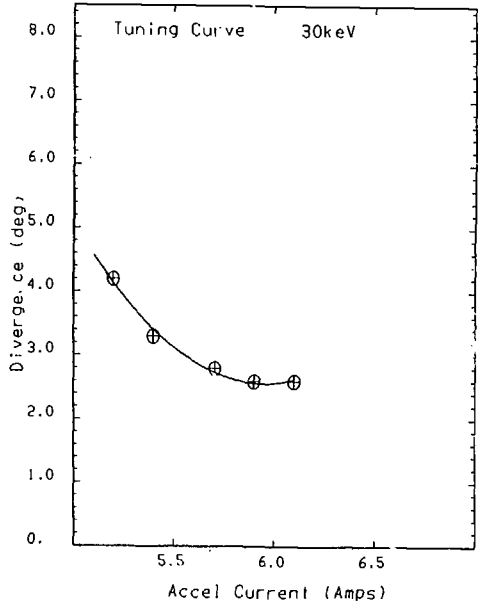

XBL 824-9352

Figure 26d

Appendix B

Computer Solution to Poisson's Equation

We will describe here our solution to Eq. 2.7. This is known in the literature as the Tonks-Langmuir plasma sheath equation.[3] Here is the equation.

$$\frac{1}{\beta^2}\ \nabla^2 x \ = \ \frac{1}{y}\ \int_0^y \frac{y'g(y')dy'}{(x(y)-x(y'))^{1/2}} - e^{-x(y)} + R\ g(y) \quad (B_1)$$

Most of the difficulty arises in evaluating the integral. Several tricks are necessary. First we interchange the dependent and independent variables (recall that we are in cylindrical coordinates and $\nabla^2 = \frac{1}{y}\frac{d}{dy} + \frac{d^2}{dy^2}$)

$$\frac{1}{\beta^2}\left[\frac{1}{y(x)}\ \frac{\partial y^{-1}}{\partial x} - \frac{\partial y^{-3}}{\partial x}\ \frac{\partial^2 y}{\partial x^2}\right] =$$

$$\frac{1}{y(x)}\ \int_0^x \frac{y(x')\ \frac{\partial y(x')}{\partial x}\ g(y(x'))\ dx'}{(x - x')^{1/2}} \quad -e^{-x} + R\ g(y(x)) \quad (B_2)$$

This simplifies the denominator of the integrand. Next, following the approach of Chun-Fai Chan[23] in solving the equation for the planar case, we introduce a change of variable; $x = t^2$.

$$\frac{1}{\beta^2}\left[-2t\left(\frac{\partial y}{\partial t}\right)^{-3}\left(\frac{\partial^2 y}{\partial t^2}\right)+2\left(\frac{\partial y}{\partial t}\right)^{-2}+\frac{2t}{y(t)}\left(\frac{\partial y}{\partial t}\right)^{-1}\right] =$$

$$\frac{1}{y(t)}\int_0^t \frac{y(t')\,\frac{\partial y(t')}{\partial t}\,g(y(t'))dt'}{(t^2-t'^2)^{1/2}} - e^{-t^2}+R\,g(y(t)) \qquad (B_3)$$

This is necessary to eliminate a singularity in the slope at the origin. We know from the approximate solution (see Appendix C) at the origin that $y \to bx^{1/2}$ and $\frac{\partial y}{\partial t} \to bx^{-1/2}$. With this change of variable $y \to bt$ and $\frac{\partial y}{\partial t} \to b$ which is regular at the origin. Because the integrand is singular at one of the end points of the integration a simple method such as the trapezoid rule will produce serious error. We treat it by taking $y(t)\frac{\partial y}{\partial t}g(y(t))$ to be constant over a small interval and explicitly integrating the remainder. To be more specific, let us introduce a mesh on the solution as shown in Fig. 27. The mesh is composed of steps of size h. We assume we know all the values y_m corresponding to all the $t_m = m\,h$, and we will compute the next unknown value of y, i.e., y_{m+1}. Eq. B3 at y_{m+1}, t_{m+1} is

$$\frac{1}{\beta^2}\left[-2(m+1)h\left(\frac{\partial y_{m+1}}{\partial t}\right)^{-3}\left(\frac{\partial\, y_{m+1}}{\partial t^2}\right)+2\left(\frac{\partial y_{m+1}}{\partial t}\right)^{-2}+\right.$$

$$\left.\frac{2(m+1)h}{y_{m+1}}\left(\frac{\partial y_{m+1}}{\partial t}\right)^{-1}\right] = \frac{1}{y_{m+1}}\int_0^{(m+1)h} \frac{y(t')\,\frac{\partial y_{m+1}}{\partial t}\,g(y(t'))\,dt'}{[((m+1)h)^2-t']^{1/2}}$$

$$-e^{-((m+1)h)^2}+R\,g(y_{m+1}) \qquad (B_4)$$

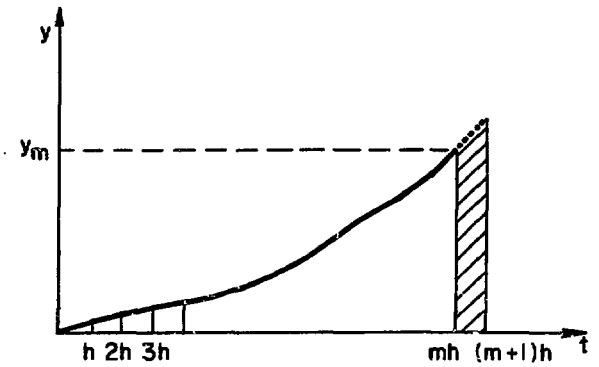

XBL824-3759

Figure 27

We convert the integral to a sum, and let $\bar{y}_n$ be the value of y at the midpoint of the interval and we take $\frac{\partial Y}{\partial t}_n = \frac{Y_{n+1}-Y_n}{h}$ to be the derivative at the midpoint on that interval.

$$\int_0^{(m+1)h} \frac{y(t')\ \frac{\partial y(t')}{\partial t}\ g(y(t')\ dt'}{((m+1)h)^2 - t'^2)^{1/2}} = \sum_{n=1}^{(m+1)} \bar{y}_n \frac{\partial y_n}{\partial t}\ g(\bar{y}_n) \times \int_{(n-1)h}^{nh} \frac{dt'}{((m+1)h)^2 - t'^2]^{1/2}}$$

$$= \sum_{n=1}^{m+1} \bar{y}_n \frac{\partial y_n}{\partial t}\ g(\bar{y}_n) \left[\sin^{-1}\left(\frac{n}{m+1}\right) - \sin^{-1}\left(\frac{n-1}{m+1}\right)\right] \qquad (B_5)$$

All the elements of the sum are known except the last (m+1) one. We do not the values of the terms dependent only because we do not know y_{m+1} yet. We will call $\frac{\partial y}{\partial t}=f$. The left hand side of equation B4 is usually small and it is most instructive to examine the equation with the left hand side equal to zero. If we multiply through by y_{m+1}, we have

$$0 = \sum_{n=1}^{m} \bar{y}_n \frac{\partial y_n}{\partial t}\ g(\bar{y}_n) \left[\sin^{-1}\left(\frac{n}{m+1}\right) - \sin^{-1}\left(\frac{n-1}{m+1}\right)\right]$$

$$+ (y_m + \frac{h}{2}f)\ f g(\bar{y}_{m+1}) \left[\pi/2 - \sin^{-1}\left(\frac{m}{m+1}\right)\right]$$

$$-(y_m + hf)\ e^{-((m+1)h)^2} + (y_m + hf)\ R\ g(y_{m+1}) \qquad (B_6)$$

We have substituted $y_m + hf$ for y_{m+1} and $y_m + \frac{h}{2}f$ for y_{m+1}. If we guess a value for y_{m+1} to be used in g then we have a quadratic equation in f which can be easily solved. This value of f gives us y_{m+1} and the process can be repeated. As the solution progress along in y the coefficients in the quadratic equation will change. Written as a simple quadratic

$$0 = af^2 + bf + c$$

$$a = \frac{h}{2}\, g\left[\frac{\pi}{2} - \sin^{-1}\left(\frac{m}{m+1}\right)\right]$$

$$b = y_m\, g\left[\frac{\pi}{2} - \sin^{-1}\left(\frac{m}{m+1}\right)\right] - he^{-(m+1)^2h^2} + hRg$$

$$c = Sum - y_m e^{-(m+1)^2h^2} + y_m Rg \qquad (B_7)$$

At t=o we find b starts positive and c starts negative. Both approach zero as the solution progresses. The first coefficient, a, is small and always positive. Three cases are possible, (1) c goes through zero before b, (2) b goes through zero before c, and (3) b is zero when c is zero. In case 1 the positive solution for f, which is the physical one, tends to zero. This is the pre-sheath region where the potential starts to roll over and the ions are accelerated to the Bohm velocity.[24] (Remember that f is related inversely to $\frac{\partial X}{\partial y}$). Since we have dropped the Poisson term the solution becomes nonphysical for positive c, i.e. f becomes negative. In case 2 b goes to zero. This happens because the source, g, goes to zero so a also goes to zero and the entire

expression becomes less than zero. Physically this means that the electron density is trying to exceed the ion density. It results from picking non-physical conditions at the origin such that the ions cannot free-fall continously out of the system. In case 3 no pre-sheath is formed and the electron density never exceeds the ion density but the mean ion velocity equals the Bohm velocity at that value of y (y_B) and exceeds that velocity for larger values of y. The solution will extend to infinity for this case. The same cases arise in the fluid calculation. We need to add the Poisson term to see what happens.

The Poisson term will change the equation from third order to sixth order in f but it can still be written as $S(f)=0$. In case 1 instead of f becoming negative it stays positive and approaches zero forming the sheath. Case two is unchanged. For case 3 and $y<y_B$ b8 has only one positive solution but for $y>y_B$ B8 has two possible solutions. One is identical to the solution without the Poisson term. The other is a sudden decrease in f and is the forming of the sheath. The sheath forms relatively abruptly because there is no pre-sheath, since the ion velocity is already greater than the Bohm velocity. This sheath can begin at any point $y > y_B$. The solution is double valued at every point so there are an infinite number of possible solutions. We pick the one that puts the sheath where we know the wall to be. The solution seems to change abruptly because of the size of the step used in solving the equation. $\Delta y \sim \lambda_d$ and in order to get a detailed solution within the sheath one needs a step $\Delta y \ll \lambda_d$. As we decrease the step size in our solution the difference between the two slopes becomes less.

APPENDIX C1

Approximate Solution

The solution of Eq. 2.7 near the origin with the Poisson term neglected is given by Self.[6] It is of the form

$$y = b_0 x^{1/2}(1 + b_1 x + b_2 x^2 \ldots)$$

Here we have made the substitution $x = t^2$

$$y = b_0 t(1 + b_1 t^2 + b_2 t^4 \ldots)$$

If we plug this in to 2.7 and take the beam to be uniform at the center then equate terms of the same order in t, we obtain

$$t: \quad \frac{4b_0^2}{\beta^2} = b_0^3(b_0^2 g(o) - b_0 + R\, g(o) \equiv b_0^3 A$$

$$t^3: \quad \frac{8\, b_0 b_1}{\beta^2} = b_0^3 B + 9\, b_0^2 b_1 A$$

$$B \equiv \frac{4}{3} g(o)\, b_0 b_i - (b_1 - b_0) + R\, b_i$$

$$t^5: \quad \frac{1}{\beta^2}(12 b_1^2 - 8 b_2 b_0) = b_0^3 C + 9 b_0^2 b_1 B + (15 b_0^2 b_2 + 27 b_0 b_2^2) A$$

$$C \equiv \frac{8}{5} g(o)\,(2 b_0 b_2 + b_1^2) - \frac{b_0}{2} - b_1 + b_2 + R b_2$$

Solving for the first three b's

$$b_0: \quad 0 = b_0^3\, g(o) + b_0^2\,(g(o)\,R - 1) - 4/\beta^2$$

$$b_1: \quad b_1 = \frac{-b_0}{\frac{8g(o)}{3} - 1 + R + \frac{24}{\beta^2 b_0^2}}$$

$$b_2: \quad b_2 = \frac{\frac{201\, b_1^2}{\beta^2} - b_0^3\left(\frac{8}{5}\, g(o)\, b_1^2 - \frac{b_0}{2} + b_1\right)}{b_0\left(\frac{16}{5}\, b_0^3\, g(o) - b_0^2 + b_0^2\, R + \frac{23}{\beta^2}\right)}$$

APPENDIX D

Miscellaneous Calculations

Plasma produced by electron ionization compared to plasma produced by beam ionization

In order to determine the importance of thermal ionization as a plasma production mechanism in our plasma we will compare the rates of plasma production for thermal and beam ionization.

For the beam $\frac{\partial n_i}{\partial t} = n_b \, v_b \, n_g \, \sigma_i$

where n_b = beam density

v_b = beam velocity

n_g = neutral gas density

σ_i = ionization cross sectiuon for fast particles on neutral gas

By thermal ionization $\frac{\partial n_i}{\partial t} = n_e \, n_g S$

$$\text{where } S = \frac{10^{-5} \, (T_e/E)^{1/2}}{(E)^{3/2} \, (6 + T_e/E)} \exp \left[-E/T_e\right] \text{ cm}^3/\text{sec}$$

E is the ionization energy.

n_e = electron density

Taking the ratio of these rates $R = \frac{n_b \, v_b \, \sigma_i}{n_e \, S}$

At a point 30 cm downstream for a 25 keV, 4 A beam

$$v_b = \sqrt{\frac{2E}{m}} = 10^6 \sqrt{\frac{2 \times 2.5 \times 10^4}{1}} = 2.2\ 10^8\ cm/sec$$

$$n_b = \frac{I}{ev_b A} = \frac{4}{(1.6 \times 10^{-19})(2.2 \times 10^8)(50)} = 2.2\ 10^9\ cm^{-3}$$

For the process $\overset{*}{H}^+ + H_2 \rightarrow \overset{*}{H}^+ + H_2^+ + e \quad \sigma_i = 4.5 \times 10^{-16}$

and with E = 15.2 $\quad S = 5\ \ 10^{-12}\ ,\ 6\ \ 10^{-10}$

for $\quad T_e = \ 2$ eV , 5 eV respectively.

So for $n_e \sim 10^{11}$ with perhaps 10% in a hot tail at 5 eV

$$R_2 = \frac{(2.2\ \ 10^9)(2.2\ \ 10^8)(4.5\ \ 10^{-16})}{10^{11} \qquad (5\ \ 10^{-12})} = 435$$

$$R_5 = \frac{(2.2\ \ 10^9)(2.2\ \ 10^8)(4.5\ \ 10^{-16})}{10^{10} \qquad (6\ \ 10^{-10})} = 36.3 \text{ which is much greater than 1}$$

Negative Ions

Recently articles[25] have appeared presenting evidence and theory for the production of negative ions in the volume of a plasma discharge. The process of formation is believed to be as follows. The high energy electrons (60 eV) that ionize the gas to create the plasma also excite electronic states in the neutral gas molecules. These electronic states decay into vibrational states. Thermal

electrons around one eV can then combine with the molecules in the process of dissociative attachment to form negative ions. In our plasma there are no high elergy electrons but the 25 keV beam of ions can act in the same way as the electrons. In order to estimate the magnitude of the relative density of negative ions to the density of electrons we will take a specific calculation for a particular discharge and simply replace the fast electrons with beam ions.

	Discharge (Hiskes et al)[25]	beam-generated
gas density	4.10^{14} cm^{-3}	10^{14} cm^{-3}
electron temperature	1 eV	1 eV
electron density	$2\ 10^{10}$ cm^{-3}	$8\ 10^{10}$ cm^{-3}
fast electron density	$2\ 10^{7}$ cm^{-3}	-
and energy	60 eV	-
Ion beam density	-	$2.2\ 10^{9}$ cm^{-3}
and energy	-	25 keV

The rate of formation of negative ions is proportional to the rate of formation of vibrationally excited molecules. For the discharge this is given by

$$\frac{\partial n_o^*}{\partial t} = n_o\, n_{ef}\, v_{ef}\, \sigma_e$$

so for the beam it will be

$$\frac{\partial n_o^*}{\partial t} = n_o\, n_b\, v_b\, \sigma_i$$

which means the beam is a stronger source of vibrational states by a factor of

$$F_s = \frac{n_b v_b \sigma_i}{n_{ef} v_{ef} \sigma_e} \sim 150$$

Our n_o is lower by a factor of 4 so we should create about 40 times more negative ions. However, the ion beam also introduces two destruction mechanisms not important in the discharge. Beam ions can knock off the extra electron or it can remove the electron by charge exchange. In the discharge the dominant loss is recombination.

$$\left(\frac{\partial n_i^-}{\partial t}\right)_{loss} = n_i^- n_+ \langle \sigma v_{ii} \rangle + n_i^- n_b(\sigma_{cx} + \sigma_o)$$

$$= n_i^-[(8.10^{10})(2.10^{-7}) + 5.10^{17}\ (3.10^{-15} + 6.10^{-15})]$$

$$= n_i^-\ 2.10^4$$

This is about 4 times the loss rate of the discharge. So in total we expect our system to have a net negative ion population 10 times larger than the discharge. Hiskes, et. al. report a few percent negative ions so it is possible that there could be 10% negative ions in the neutralizer. Bearing in mind that the uncertainty in this calculation is great because several cross sectic are not well known, the result suggests that further study is warranted.

Appendix E

Crossection data and other model inputs

Table 1 lists all the necessary cross sections for computing the ion production rates at 25keV. Those with * are inferred from similar processes while the rest are actual measurements. Since the original beam is composed of a mix of H^+, H_2^+, and H_3^+ ions, at the point of interest there will be those ions and all possible products from collisions with the gas. A certain fraction will have become neutral and the molecular ions will break into fragments. The extent of this will depend on the gas target thickness traversed by the beam. In addition the ions, neutrals and fractional speed fragments all have different ionization and charge exchange rates. Given a starting beam composition, say 50% H , 30% H_2^+, 20% H_3^+, a program calculates the beam composition as a function of target thickness. The beam composition is then combined with the cross sections in the table to give the total H_2^+ production, the H_2^+ production by charge exchange, and the H^+ production in the background gas. Fig. 28 presents a normalized ion density verses pressure measured 30 cm downstream. The target thickness is related to the pressure by assuming the pressure varies linearly down the neutralizer and is zero at the end of the neutralizer. The ion density is normalized so that when multiplied by the I/eV_bA at the exit of the accelerator it gives the ion

Table 1. Relavent cross sections for plasma production by ion and neutral beams on H_2 target. All cross sections are in units of 10^{-16} cm^{-3}

Slow Product	Incident Particle	Cross section for ionization at energy (keV) 25	16.6	12.5	8.3	Cross section for charge exchange at energy (keV) 25	16.6	12.5	8.3
H_2^+	H^+	1.5		1.2	.9	4.8		8.0	8.6
	H^0	1.2		1.0	.6				
	H_2^+	1.2*	.9*			3.0	4.0		
	H_2^0	1.3	1.1						
	H_3^+	.9*							
H^+	H^+	1.0		1.0	.9				
	H^0	.18		.12	.08				
	H_2^+	1.0*	.8*						
	H_2^0	.53	.4						
	H_3^+	.8*							

* Cross section inferred from similar process.

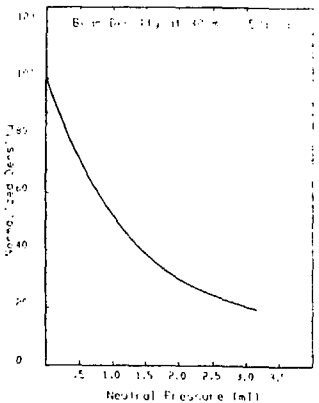

Figure 28a

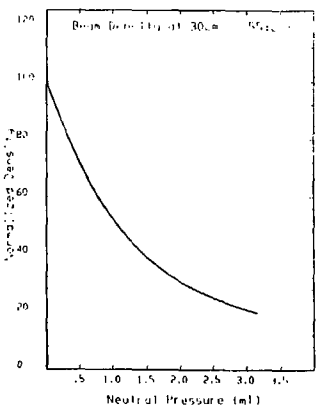

Figure 28b

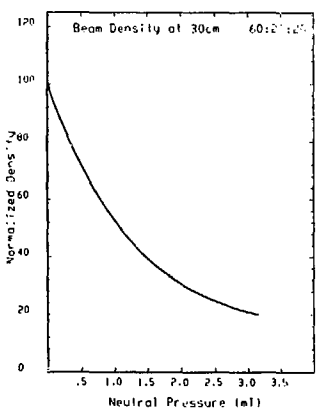

XBL 825-9842

Figure 28c

density of the beam 30 cm downstream. The cross section (Fig. 29) is normalized so that the expression $\frac{I_{acc}\, n_g\, \sigma_{eff}}{eA}$ gives the total H_2^+ production 30cm downstream.

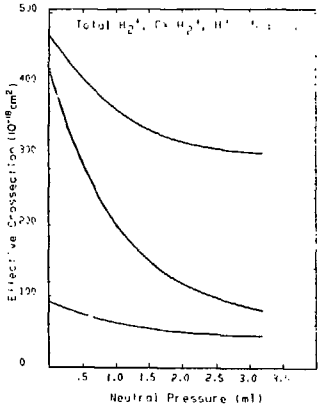

Figure 29a

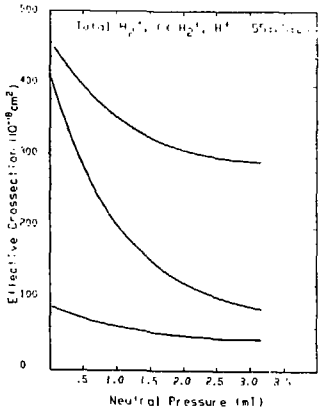

Figure 29b

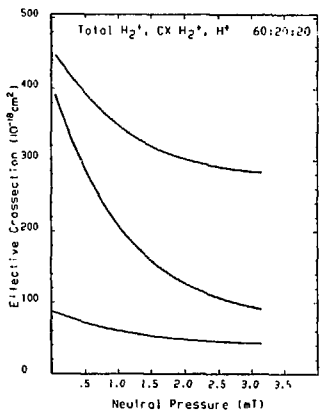

XBL 825-9841

Figure 29c

APPENDIX F

Computer Program Listing

```
      PROGRAM AUTOSEL
C
      DIMENSION T(1000),V(1000),IDATE(9)
      DIMENSION DEN(2000),E(1000),YPLOT(2000),IPARM(11)
      REAL*8 Y,C(7),PARAMS(10),YP,R,VTMP,TZ,ERF,RSCALE,SUMFST,SUMFL,
     . EFAST,VBAR,DEL,PMN,PMO,BMSHP,YNW,Y1P,Y2P,EPR
      REAL*8 BETA,B2,RNBNE,RB,EPS,GUESS,ROUT,A2,A3,B,CC,QQ,RPHIT,RVTSC,
     .Q,SUM,Q1,PQ1,ASO,ASN,RNEE,H,HALFPI,WD,GY,GYAVE,YNEW,YAVE,VALUE,RIN
      INTEGER FILEAA
C
      COMMON /INT/ Y(1000)
C
      DEFINE FILE 20(7,4010,U,FILEAA)
C
      DATA EGBC,EMASS/1.6E-19,9.11E-28/
      DATA IOP,IOW,LP/3,6,7/
      DATA IPARM/'NETEPRNBDVEFRVWPRIEI  '/
      DATA HALFPI/1.5707963267949D0/
C
      YP(I,R)=(Y(I+1)-Y(I))/R
C
      CALL DATTIM(IDATE)
      WRITE(LP,502) IDATE
502   FORMAT(2X,9A2)
1001  WRITE(6,105)
105   FORMAT('  ENTER NUMBER OF TRACES')
      READ(3,*) NPLOT
      IF(NPLOT) 730,1000,
      WRITE(6,104)
104   FORMAT(//,3X,'ENTER PARAMETER TO BE VARIED: NE,TE,PR,NB,DV,EF,RV,
     . WP')
      READ(3,106) IPM
106   FORMAT(A2)
      DO 107 I=1,11
107   IF(IPM.EQ.IPARM(I)) JPRM=I
      IPLOT=0
      ML1=0
      INFS=0
C
C Parameters are entered in real units and converted to
C   computer units.
C
101    WRITE(6,102)
102    FORMAT(' '/' ENTER NE (10E10), Te (eV), PRODUCTION RATE '
     .,'(10e16 CM-3/SEC)',/,' Nbeam (10e10), BEAM DIVERGENCE (DEG),'
     .,' AVERAGE FAST ION ENERGY, RATIO PHI/T,',/,' SHEATH START #,',
     . ' RATIO TOTAL PRODUCTION/IONIZATION RATE,'/,
     . ' ELECTRON IONIZATION RATE (No*Ve*Sigma*10e6), BEAM SHAPE #')
      READ(3,*) PARAMS,ISHAPE
      IF(PARAMS(1).LT.0.) GO TO 1001
      WRITE(6,103)
103   FORMAT(' ENTER STEP SIZE, # OF STEPS, EPS, NSTART')
      READ(3,*) H,ML,EPS,NST
      NNST=NST
      PMO=PARAMS(JPRM)/2.D0
      IF(JPRM.EQ.3) PMO=PMO+PARAMS(JPRM)
1002  WRITE(13,1007) IPARM(JPRM),PARAMS(JPRM)
```

```
1007    FORMAT(5X,A2,' = ',F20.14)
        RSCALE=.979D0*PARAMS(1)*SQRT(PARAMS(2)    )/PARAMS(3)
        TZ=PARAMS(5)*60.D0*HALFPI/90.D0/RSCALE
        B2=RSCALE*RSCALE/(552049.D0*PARAMS(2)/PARAMS(1))*10.D0**10.D0
        RNBNE=PARAMS(4)/PARAMS(1)
        RPHIT=      PARAMS(7)
        WD=3.5D0/RSCALE
        INFS=1
        IF(PARAMS(6).EQ.0.) INFS=0
C THE 2 BELOW IS FOR H INSTEAD OF B2
        EFAST=    PARAMS(6)/(PARAMS(2)*H*H)
        RVTSC=1.D0-1.D0/EXP(RPHIT)
        ISHETH=PARAMS(8)
        EPR=PARAMS(1)*PARAMS(10)/PARAMS(3)
        WRITE(13,500) PARAMS,H,ML,EPS,NST
        WRITE(LP,500) PARAMS,H,ML,EPS,NST
500     FORMAT('     Ne= ',E8.2,'  Te= ',F4.1,' PR0',E8.2,'  Nb= ',E8.2,
     .'BEAM DIVERGENCE= ',F4.1,'DEG.','AVERAGE FAST ION ENERGY= ',F4.1,/
     .,'RATIO PHI/Te = ',F4.1,' SHEATH START # ',F4.1,' PRODUCTION RATI
     .0 =',F4.1,' ELECTRON PRODUCTION =',F4.2,/
     .,'   STEP SIZE=',E8.2,'   '
     .,I4,' STEPS   EPS=',E8.2,'   NSTART=',I4)
        IF(ML.EQ.0 ) GO TO 1000
C
C The solution near the origin is calculated from an expansion
C   and used for the first few steps.
C
        SUM=0.D0
        IF(INFS.EQ.0) GO TO 603
        ASO=0.D0
        SUM=WD/(5.D0*SQRT(EFAST*2.D0)*H)
C
603     C(1)=(-4.D0)/B2
        C(2)=0.D0
        C(3)=BMSHP(0.D0,WD,TZ,ISHAPE)*RNBNE-1.D0+SUM
        C(4)=BMSHP(0.D0,WD,TZ,ISHAPE)+EPR
        GUESS=-C(3)/C(4)
        CALL NWTN3D(ROUT,GUESS,C,EPS)
        A2=ROUT*ROUT
        A3=ROUT*A2
        GUESS=BMSHP(0.D0,WD,TZ,ISHAPE)
C
      B=ROUT*(-1.D0-2.D0*EPR*A2/3.D0)/(8.D0*ROUT*(GUESS+EPR)/3.D0
     .-1.D0+RNBNE*GUESS+24.D0/
     .(B2*A2))
C
        CC=(201.D0*B*B/B2-A3*(1.6D0*B*B*(GUESS+EPR)
     .-(ROUT/2.D0-B)+8.D0*EPR*(4.D0*ROUT*B+A2/2.D0)/15.D0))/(ROUT*(
     .  3.2D0*A3*(GUESS+EPR) -A2+A2*RNBNE*GUESS+23.D0/B2))
C
        DO 20 I=1,NST
        II=1+ML1*IPLOT
        Y(II)=ROUT*H*(I-1.D0)+B*(H*(I-1.D0))**3.D0+CC*(H*(I-1.D0))**5.D0
        T(II)=H*(I-1.D0)
        V(II)=(H*(I-1.D0))**2.D0*PARAMS(2)
        IF(I.NE.1) E(II)=(V(II)-V(II-1))/(Y(II)-Y(II-1))/RSCALE
        DEN(I+2.*ML1*IPLOT)=PARAMS(1)*((1.-EXP(T(II)*T(II)-RPHIT))/
     . (EXP(T(II)*T(II))*RVTSC))
        DEN(I+ML+2*ML1*IPLOT)=DEN(I+2.*ML1*IPLOT) - RNBNE*PARAMS(1)
        WRITE(LP,501) I,Y(II),V(II),DEN(I+ML+2*ML1*IPLOT),
     .DEN(I+2*ML1*IPLOT)
20      CONTINUE
        E(1+ML1*IPLOT)=0.
        WRITE(6,*) B2,TZ,RNBNE,RSCALE
```

```
      WRITE(6,*) ROUT,B,CC,SUM
      WRITE(9,*) WD,TZ
      RIN=ROUT
      CS=1.D0
      Q=1.D0
      FLUXI=0.D0
      FLUXE=0.D0
      IWALL=1
C
C The main loop begins here.
C
720   DO 100 IM=NST,ML
      M=IM
90    MMM=M+ML1*IPLOT
      SUM=0.D0
      ISHOOT=0
      VBAR=0.D0
      SUMFST=0.D0
      ASO=0.D0
      Q=FLOAT(M)
C
C SMFAST and SUMINT calculate the integrals for the fast and
C   slow ions.  SUMELE calculates the contribution for electrons.
C
C Add Fast Ions
C
      JST=MMM+2-M
      IF(INFS.EQ.0) GO TO 599
      CALL SMFAST(SUMFST,Q,JST,MMM,WD,TZ,H,EFAST,ISHAPE)
      SUMFST=SUMFST/(5.D0*SQRT(2.D0))
      SUMSAV=SUMFST
      ASO=0.D0
C
C Add electron contribution
C
599   IF(EPR.EQ.0.) GO TO 600
      CALL SUMELE(SUM,Q,JST,MMM,WD,TZ,H,ASO,VBAR,RPHIT,RVISC,EPR)
      ASO=0.D0
C
600   CALL SUMINT(SUM,Q,JST,MMM,WD,TZ,H,ASO,VBAR,ISHAPE)
C
      VTMP=Q*Q*H*H
C     RNEE=Y(MMM)*( 1.D0 /EXP(VTMP))
C  Electron density distribution including effect of potential well.
      RNEE=Y(MMM)*(1.D0-1.D0/EXP(RPHIT-VTMP))/(EXP(VTMP)*RVTSC)
C
15000 YNEW=Y(MMM)+H*ROUT
      YNW =1.25D0*Y(MMM)-.3125D0*Y(MMM-1)+.0625D0*Y(MMM-2)
C     Y1P=(-163.D0*Y(MMM)/60.D0+5.D0*Y(MMM-1)-10 D0*Y(MMM-2)/3.D0 +
C    .  5.D0*Y(MMM-3)/4.D0 - .2D0*Y(MMM-4))/H
      Y1P=YP(MMM-1,H)
C     Y2P=(-191.D0*Y(MMM)/12.D0+205.D0*Y(MMM-1)/6.D0-85.D0*Y(MMM-2)
C    . /3.D0 + 12.25D0*Y(MMM-3) -13.D0*Y(MMM-4)/6.D0)/(H*H)
      Y2P=(-46.844715D0 *Y(MMM)/3.D0+100.32977D0 *Y(MMM-1)/3.D0-83.1081
     .7D0 *Y(MMM-2)/3.D0+11.964595D0*Y(MMM-3)-6.3437D0  *Y(MMM-4)/3.D0)
     ./(H*H)
      YAVE=.3125D0*H*ROUT+YNW
      GYAVE=BMSHP(YAVE,WD,TZ,ISHAPE)
      IF(GYAVE.GT..1 ) IFST=MMM
      GY=BMSHP(YNEW,WD,TZ,ISHAPE)
      SUMFL=0.D0
      IF(INFS.NE.0)
     . SUMFL=      (ARSIN((YAVE/YNEW)*SQRT(EFAST/(EFAST+Q-.25D0))
     .   )/HALFPI-1.D0)/(5.D0*SQRT(EFAST*2.D0))
```

```
C
C       C(1)=SUM-RNEE + RNBNE* Y(MMM   *GY + Y(MMM)* SUMFST
        C(1)=SUM
C       C(2)=Y(MMM)*(HALFPI-ASO)
        C(2)=          HALFPI-ASO
C       C(3)=-H*RNEE/Y(MMM)
        C(3)=   RNEE/Y(MMM) - SUMFST
C       C(4)=RNBNE*H
        C(4)=RNBNE
C       C(5)=H*(HALFPI-ASO)/2.D0
        C(5)=H*SUMFL
        C(6)=2.D0/B2
        C(7)=EPR*C(2)*RNEE/Y(MMM)
C
        RIN=(3.875D0*Y(MMM-57.25D0*Y(MMM-1)/6.D0+9.375D0*Y(MMM-2)
     .-4.625D0*Y(MMM-3)+11.D0*Y(MMM-4)/12.D0)/H
        IF (Q.LT.20) RIN=ROUT
        IF(RIN.LT.0.) RIN=-2.D0*RIN
        RIN=RIN*1.5D0
        IF(M.GT.ISRETH) RIN=1.D0
C       CALL NWTNF1(ROUT,RIN,C,EPS,YNW,Y(MMM),H,WD,TZ,ISHAPE)
15005   CALL NWTNF3(ROUT,RIN,C,EPS,YNW,Y(MMM),Y1P,Y2P,Q,H,WD,TZ,ISHAPE)
C       CALL NWTN5D(ROUT,RIN,C,EPS)
        WRITE(8,*) C(1),C(2),C(3),ROUT
        WRITE(9,*) C(1),C(2),C(3),C(6),YNW,Y(MMM),Y1P,Y2P,Q,ROUT,RIN
C
        Y(MMM+1)=Y(MMM)+H*ROUT
        YAVE=Y(MMM)+H*ROUT/2.D0
        GYDEN=BMSHP(YAVE,WD,TZ,ISHAPE)
        YDYDT=(Y(MMM+1)-Y(MMM))*YAVE/H
       DEN(MMM+IPLOT*ML1)=PARAMS(1)*(1.D0-1.D0/EXP(RPHIT-VTMP))/(EXP(VTMP
     .          )+RVTSC)
        DEN(MMM+1+ML+IPLOT*ML1)=PARAMS(1)*(SUM+YDYDT*(HALFPI-ASO)*(GYDEN
     .+EPR*DEN(MMM+IPLOT*ML1)/PARAMS(1)))/Y(MMM+1)
        GYDEN=GYDEN*YDYDT*H
        FLUXI=(VBAR+GYDEN)/Y(MMM+1)
        IF(INFS.NE.0) FLUXI=1.2*FLUXI
        VBAR=FLUXI/DEN(MMM+1+ML+IPLOT*ML1)
        IF(ROUT.GT.RIN) VBARS=VBAR*PARAMS(1)
C
C Various useful quantles such as potential, electric field, and
C   electron and ion densities are calculated and put in real
C   units.
C
        T(MMM)=(Q-1.D0)*H
        VTMP=T(MMM)*T(MMM)
        V(MMM)=       VTMP*PARAMS(2)
        E(MMM)*(V(MMM)-V(MMM-1))/(Y(MMM)-Y(MMM-1))/RSCALE
C       WRITE(6,513) SUM,RNEE,ROUT,Y(MMM+1),GYAVE,SUMFST,SUMFL,VBAR
        CHRG=DEN(MMM+ML+IPLOT*ML1)-DEN(MMM+IPLOT*ML1)
        CENT=(C(1)+C(2)*ROUT+C(3)*ROUT*ROUT)/(Y(MMM)*ROUT**3)
        DIFF=CENT-CHRG
C       WRITE(6,*) DIFF,CENT,CHRG
        IF(ROUT.LT.0.AND.JPRM.NE.11) GO TO 1111
        IF(ROUT.GT.10000.AND.JPRM.NE.11) GO TO 1111
513     FORMAT(7(3X,D9.4))
        WRITE(LP,501) M,Y(MMM),V(MMM),SUM,RNEE
501     FORMAT(' STEP',I4,' R=',F8.5,'  V=',F7.4,'     ION DENSITY='
     .,E9.3,'     ELECTRON DENSITY=',E9.3)
        FLUXI=FLUXI/PARAMS(9)
        FLUXE=31.5*DEN(MMM+IPLOT*ML1)/(SQRT(HALFPI)*PARAMS(1))
        IF(FLUXE.GT.FLUXI) IWALL=MMM
100     CONTINUE
C
```

```
C Next section provides automatic variation of parameters to
C   find solution that extends to infinity.
C
      GO TO 1112
1111  DEL=(     PARAMS(JPRM)-PMO)/2.D0
      IF(     ABS(DEL) .LT..1*EPS) GO TO 1114
      PARAMS(JPRM)=PMO + DEL
      GO TO 1002
1114  PARAMS(JPRM)=PMO
      GO TO 1002
1112  IF(JPRM.EQ.11) GO TO 1113
      PMN=PARAMS(JPRM) + (PARAMS(JPRM)-PMO)/2.D0
      PMO=PARAMS(JPRM)
      IF(ABS(PMN-PMO).LT..09*EPS) GO TO 1113
      PARAMS(JPRM)=PMN
      GO TO 1002
C
C113  CALL CHECK(MMM-ML+1,MMM,B2,H)
1113  II=1+ML1*IPLOT
      DO 1850 I=II,MMM
1850  YPLOT(I)=Y(I)*RSCALE
      IF(IPLOT+1.EQ.NPLOT) GO TO 40
      ML1=ML
      IPLOT=IPLOT+1
      GO TO 101
40    IF(NPLOT.EQ.1) ML1=ML
730   NPLOT=ABS(NPLOT)
      CALL ERASE
C     Terminal display of results
      CALL PLTALL(YPLOT,T,ML1+ML*IPLOT,1,1,ML1)
      WRITE(6,*) B2,TZ,RNBNE,RSCALE
      WRITE(6,509) YPLOT(IWALL),V(IWALL),DEN(IWALL),VBARS
509   FORMAT(20X,' WALL POSITION IS ',F6.3,/,20X,' POTENTIAL IS ',F4.2,/
     .20X,' ELECTRON DENSITY IS ',F4.2,/,20X,' NORMALIZED ION VELOCITY='
     .,' ',F5.3,/////,' NEW ENDPOINT?  (IN I3)')
      READ(3,510) NML
510   FORMAT(I3)
      IF(NML.EQ.0) GO TO 710
      IF(NML.LE.ML) GO TO 701
702   NST=ML
      ML2=2*ML
      DO 705 L=1,ML
705   DEN(NML+ML+1-L)=DEN(ML2+1-L)
      ML=NML
      GO TO 720
701   ML1=NML
      WRITE(6,512)
512   FORMAT(' FIX DENSITY?')
      READ(3,511) IDEN
511   FORMAT(I1)
      IF(IDEN.EQ.0) GO TO 730
      DO 706 L=1,NML
706   DEN(NML+L)=DEN(ML+L)
      ML=NML
      GO TO 730
710   CALL PLTALL(YPLOT,V,ML1+ML*IPLOT,1,1,ML1)
      CALL PLTALL(YPLOT,E,ML1+ML*IPLOT,1,1,ML1)
      DO 700 J=1,IPLOT
      DO 700 I=1,ML
      NN=ML+1-I+(NPLOT-J)*ML1
      MM=2*ML+1-I+(NPLOT-J)*ML1*2
      YPLOT(MM)=YPLOT(NN)
700   YPLOT(MM-ML)=YPLOT(NN)
      DO 699 M=1,ML1
```

```
699     YPLOT(M+ML1)=YPLOT(M)
        CALL PLTALL(YPLOT,DEN,(ML1+ML*IPLOT)*2,1,1,ML1)
C       CALL PLTALL(YPLOT,V,ML*2,1,1,ML)
        WRITE(6,513) PARAMS
        WRITE(6,*) PARAMS(JPRM)
        WRITE(6,*)          M,ML,EPS,NST
       READ(3,511) IHOLD
C Permanent storage of graphic results
797     WRITE(6,799)
799     FORMAT('0TO SAVE PLOT ENTER A SET #')
        READ(3,511) ISET
        IF(ISET.EQ.0) GO TO 798
        LLL=(ML1+ML*IPLOT)*2
        WRITE(20'ISET,ERR=99) (YPLOT(I),I=1,1000),(DEN(J),J=1,1000),LLL
798     ML1=ML
602    WRITE(6,800)
800    FORMAT(////,21X,'ENTER NEW PARAMETER: NE,TE,PR,NB,DV,EF,RV,WP,RI,'
     *,'EI')
803     ISURE=0
       READ(3,801) NEWPM,VALUE
        IF(VALUE.GE.100.AND.NEWPM.NE.IPARM(8)) WRITE(6,804)
804     FORMAT(' ARE YOU SURE?')
        IF (VALUE.GE.100.AND.NEWPM.NE.IPARM(8)) READ(3,511) ISURE
        IF(ISURE.NE.0) GO TO 803
801    FORMAT(A2,F16.12)
       IF(IPARM(11).EQ.NEWPM) GO TO 1001
        DO 802 I=1,10
802     IF(IPARM(I).EQ.NEWPM) PARAMS(I)=VALUE
        NST=NNST
        PMO=PARAMS(JPRM)/2.
        IF(JPRM.EQ.3) PMO=PMO+PARAMS(JPRM)
       GO TO 1002
99      WRITE(6,450)
450     FORMAT('*** DISK TRANSCRIPTION ERROR ***')
        GO TO 797
1000    ENDFILE LP
        STOP
        END
```

```
      SUBROUTINE SUMINT(SUM,Q,I1,I2,WD,TZ,H,ASO,TCUR,ISHAPE)
       REAL*8 Y,SUM,Q,WD,TZ,H,ASO,ASN,YAVE,CY,ERF,TCUR,YDYDT,RMSHP
C
       COMMON /INT/ Y(1000)
C
       QI=1.D0/Q
       PQI=0.D0
C
       DO 10 KK=I1,I2
C      YAVE=(Y(KK)+Y(KK-1))/2.D0
       YAVE=.375D0*Y(KK)+.75D0*Y(KK-1)-.125D0*Y(KK-2)
       IF(KK.   EQ.I1)  YAVE=(Y(KK)+Y(KK-1))/2.D0
       CY=RMSHP(YAVE,WD,TZ,ISHAPE)
C      YDYDT=(Y(KK)**2.D0-Y(KK-1)**2.D0)/(H*2.D0)
       YDYDT=  YAVE*(Y(KK)-Y(KK-1))/ H
       TCUR=TCUR+CY*YDYDT*H
       PQI=PQI+QI
       ASN=ARSIN(PQI)
       SUM=SUM+YDYDT*(ASN-ASO)*CY
10     ASO=ASN
      RETURN
      END
```

```
      SUBROUTINE SUMELE(SUM,Q,I1,I2,WD,TZ,H,ASO,TCUR,RPT,RVT,EPR)
       REAL*8 Y,SUM,Q,WD,TZ,H,ASO,ASN,YAVE,GY,EPR,TCUR,YDYDT,RPT,RVT
C
       COMMON /INT/ Y(1000)
C
       QI=1.D0/Q
       PQI=0.D0
C
       DO 10 KK=I1,I2
       PQI=PQI+QI
C      YAVE=(Y(KK)+Y(KK-1))/2.D0
       YAVE=.375D0*Y(KK)+.75D0*Y(KK-1)-.125D0*Y(KK-2)
       IF(KK.  EQ.I1) YAVE=(Y(KK)+Y(KK-1))/2.D0
       GY=EPR*(1.D0/EXP((PQI-QI/2.D0)**2)-1.D0/EXP(RPT))/RVT
C      YDYDT=(Y(KK)**2.D0-Y(KK-1)**2.D0)/(H*2.D0)
       YDYDT= YAVE*(Y(KK)-Y(KK-1))/ H
       TCUR=TCUR+GY*YDYDT*H
       ASN=ARSIN(PQI)
       SUM=SUM+YDYDT*(ASN-ASO)*GY
10     ASO=ASN
      RETURN
      END




      SUBROUTINE SMFAST(SUM,Q,I1,I2,WD,TZ,H,E,ISHAPE)
       REAL*8 Y,SUM,Q,WD,TZ,H,E,T2,TP2,YAVE,GY,ERF,HALFPI,YQ,TEMP
     .,BMSHP
C
       COMMON /INT/ Y(1000)
C
       DATA HALFPI/1.5707963267949D0/
       T2=Q*Q
       YQ=2.D0*Y(I2)-Y(I2-1)
       RKK=-.5D0
       SUM=SUM+WD
C
       DO 10 KK=I1,I2
       RKK=1.D0+RKK
       TP2=RKK*RKK
       YAVE=.375D0*Y(KK) + .75D0*Y(KK-1) - .125D0*Y(KK-2)
       IF(KK.  EQ.I1) YAVE=(Y(KK)+Y(KK-1))/2.D0
       GY=BMSHP(YAVE,WD,TZ,ISHAPE)
       TEMP=YAVE*SQRT(E/(E+T2-TP2))/YQ
C      IF(ABS(TEMP).GT.1.) WRITE(6,*) YAVE,YQ,E,T2,TP2,TEMP,SUM
       SUM=SUM+GY*(Y(KK)-Y(KK-1))*(ARSIN(TEMP)/HALFPI -1.D0)
10     CONTINUE
       SUM=SUM/(SQRT(E)*H)
      RETURN
      END
```

```
      SUBROUTINE NWINF3(ROUT,RIN,C,EPS,Y1,Y2,YP,Y2P,Q,H,WD,TZ,ISP)
      IMPLICIT DOUBLE PRECISION(F)
       REAL*8 C(1),ROUT,RIN,EPS,XOLD,XNEW,Z,ZP,Y1,Y2,H,WD,TZ,
     . BMSHP,DBMSHP,YP,Y2P,Q
      DIMENSION IUFT(8),IBUF(40)
        F(Z)=(Z*(C(2)*BMSHP(Y1+.3125D0*H*Z,WD,TZ,ISP)+C(7))*(Y1+.3125D0*H
     .*Z)/(Y2+H*Z) - C(3) + Z*C(5)*BMSHP(Y1+.3125D0*H*Z,WD,TZ,ISP)+
     .C(4)*BMSHP(Y2+H*Z,WD,TZ,ISP)+C(1)/(Y2+H*Z))*Z**3
     .    -C(6)*(Q*H *Z*Z                          /(Y2+H*Z) +
     .    Q*YP       +(1.D0-Q)*Z    )
      FP(Z)=((C(2)*BMSHP(Y1+.3125*H*Z,WD,TZ,ISP)+C(7))*((Y1+.3125*H*Z)
     ./(Y2+H*Z)
     .+H*Z*(.3125D0*Y2-Y1)/((Y2+H*Z)**2.D0))-H*C(1)/((Y2+H*Z)**2.D0)
     .+.3125D0*H*Z*C(2)*
     .DBMSHP(Y1+.3125D0*H*Z,WD,TZ,ISP)+C(4)*DBMSHP(Y2+H*Z,WD,TZ,ISP)*H
     .+C(5)*(BMSHP(Y1+.3125D0*H*Z,WD,TZ,ISP)+Z*H*DBMSHP(Y1+.3125D0*H*Z,
     .WD,TZ,ISP)*.3125D0))*Z*Z*Z
     .+(Z*(C(7)+C(2)*BMSHP(Y1+.3125D0*H*Z,WD,TZ,ISP))*(Y1+.3125D0*H*Z)
     ./(Y2+H*Z) - C(3) + Z*C(5)*BMSHP(Y1+.3125D0*H*Z,WD,TZ,ISP)
     .+C(4)*BMSHP(Y2+H*Z,WD,TZ,ISP) +C(1)/(Y2+H*Z))*
     . 3.D0*Z*Z
     .-C(6)*(Q*H*Z*(2.D0-Z*H/(Y2+H*Z))/(Y2+H*Z) +(1.D0-Q))                    F
      CALL INTLEN(.FALSE.)
      K=0
      CALL BLDUFT(IUFT,K,63,4ZE000)
      CALL READ4(IUFT,IBUF,80,.FALSE.)
       XOLD=RIN
1      XNEW=XOLD- F(XOLD)      / FP(XOLD)
       IF(ABS(XNEW-XOLD) .LT. EPS) GO TO 2
      IF(IAND(IUFT(1),1).NE.1) GO TO 2
       XOLD=XNEW
       GO TO 1
2      ROUT=XNEW
       CALL TRMINB(IUFT)
      RETURN
      END
```

```
      SUBROUTINE NWTN3D(ROUT,RIN,C,EPS)
       IMPLICIT DOUBLE PRECISION(F)
       REAL*8 C(1),ROUT,RIN,EPS,XOLD,XNEW,Z,ZP
      DIMENSION IUFT(8),IBUF(40)
       F(Z)=C(4)*Z**3.D0+C(3)*Z**2.D0+C(2)*Z+C(1)
       FP(Z)=3.D0*C(4)*Z**2.D0+2.D0*C(3)*Z+C(2)
      CALL INTLEN(.FALSE.)
      K=0
      CALL BLDUFT(IUFT,K,@3)
      CALL READ4(IUFT,IBUF,80,.FALSE.)
       XOLD=RIN
1      XNEW=XOLD-F(XOLD)/FP(XOLD)
       IF(ABS(XNEW-XOLD) .LT. EPS) GO TO 2
      IF(IAND(IUFT(1),1).NE.1) GO TO 2
       XOLD=XNEW
       GO TO 1
2      ROUT=XNEW
       CALL TRMIN8(IUFT)
      RETURN
      END
```

```
      DOUBLE PRECISION FUNCTION BMSHP(Y,WD,TZ,ISPARE)
C FOR ISPARE=4,5,6 BEAM SHAPE IS CONSTANT,CAUSSIAN, OR DIFFERENCE
C   OF ERROR FUNCTIONS.  FOR ISPARE 1,2,3 THE SHAPE FACTOR IS NEVER
C   LESS THAN .04.
       REAL*8 Y,WD,TZ,ERF,DUM,ARG
       GO TO (10,20,30,10,20,30,40,50),ISPARE
10     BMSHP=1.D0
       GO TO (100,100,100), ISPARE
      RETURN
20     BMSHP=1.D0/EXP(Y*Y/(WD*WD))
       GO TO (100,100,100), ISPARE
      RETURN
30     BMSHP=(ERF((Y+WD)/TZ,DUM)-ERF((Y-WD)/TZ,DUM))/2.D0
       GO TO (100,100,100), ISPARE
      RETURN
100      BMSHP=BMSHP+.15D0/EXP(Y*Y/(25.D0*TZ*TZ))                    C
       RETURN
40     BMSHP=1.D0-Y/(2.D0*WD)
       IF(BMSHP.LT.0.) BMSHP=0.
       RETURN
50     BMSHP=1.5*COS(3.14*(Y-.37*WD)/(1.5*WD))**2*(1.-Y/(2.*WD))**2
       IF(BMSHP.  LT.0.) BMSHP=0.D0
       RETURN
      END
```

```
      DOUBLE PRECISION FUNCTION DBMSHP(Y,WD,TZ,ISPARE)
C  DERIVITIVE OF BMSHP WRT Y
C FOR ISPARE=4,5,6 BEAM SHAPE IS CONSTANT,CAUSSIAN, OR DIFFERENCE
C   OF ERROR FUNCTIONS.  FOR ISPARE 1,2,3 THE SHAPE FACTOR IS NEVER
C   LESS THAN .04.
       REAL*8 Y,WD,TZ,ERF,DUM
       GO TO (10,20,30,10,20,30,40,50,60),ISPARE
10     DBMSHP=0.D0
       GO TO (100,100,100), ISPARE
      RETURN
20     DBMSHP=-Y*2.D0/(EXP(Y*Y/(WD*WD))*WD*WD)
       GO TO (100,100,100), ISPARE
      RETURN
30     DBMSHP=(EXP(-((Y+WD)/TZ)**2)-EXP(-((Y-WD)/TZ)**2))/(2.D0*TZ)
       GO TO (100,100,100), ISPARE
      RETURN
100    IF(DBMSHP.LT..04) DBMSHP=0.D0
       RETURN
40     DBMSHP=  -1.D0/(2.D0*WD)
       IF(DBMSHP.LT.0.) DBMSHP=0.D0
       RETURN
50     DBMSHP=1.5*COS(3.14*(Y-.37*WD)/(1.5*WD))**2*(1.-Y/(2.*WD))**2
       IF(DBMSHP.LT.0.) DBMSHP=0.
       RETURN
60     DBMSHP=-Y*2.D0*(1.D0/(1.859D0*WD*WD*EXP(Y*Y/(1.69D0*WD*WD))) +
     . 1.D0/(.116D0*WD*WD*EXP(Y*Y/(.04*WD*WD)))  )
       RETURN
      END
```